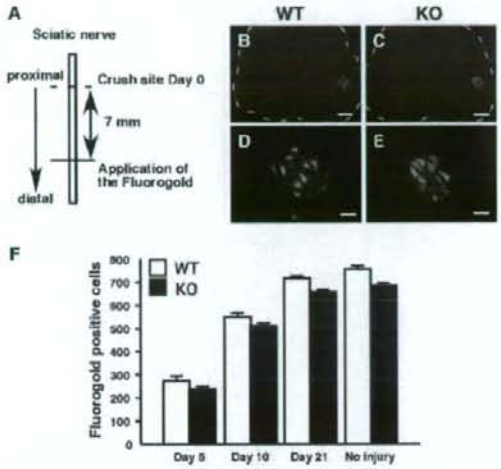

FIGURE 3. **Regenerating axons elongate normally in meltrin-β-deficient mice.** *A*, at 5, 10, and 21 days after a sciatic nerve crush, the nerve (*bar*) was crushed 7 mm distal to the lesion, and crystals of the retrograde tracer Fluorogold were applied to the cut nerve. *B–E*, sections through the ventral horn of the spinal cord that show a similar number of motoneurons labeled with Fluorogold in both genotypes of animals at 10 days after the lesion. The *dotted lines* indicate spinal cords. *Bars*: 250 μm (*B* and *C*) and 50 μm (*D* and *E*). *WT*, wild type; *KO*, knock out. *F*, the numbers of neurons labeled in retrograde are similar in both genotypes of animals. The mean ± S.E. from four wild type and three mutant deficient mice are shown.

meltrin-β-deficient mice, although the progression of the myelination recovered in the late stage of regeneration in these mice.

The delay in the early stage of regeneration in meltrin-β-deficient mice could be because of the decreased rate of axon elongation after the lesion. To evaluate the axonal regeneration rate, spinal motoneurons and DRG neurons were labeled in retrograde with Fluorogold 5, 10, and 21 days after the crush at a site 7 mm distal to the lesion (Fig. 3). Fluorogold was used as a marker because it is a long-lasting and non-diffusible tracer that undergoes rapid retrograde axonal transport (26, 28). Meltrin-β-deficient mice had similar numbers of labeled spinal motoneurons as wild type mice at any day point after the crush, suggesting that the axons of meltrin-β-deficient mice elongated over the lesion and reached the injection site as efficiently as those of the wild type mice (Fig. 3*F*). Similar results were obtained in the DRG neurons (data not shown). These results exclude primary defects of meltrin-β-deficient mice in the axonal elongation during regeneration.

Delay in Progression of Schwann Cell Differentiation in Meltrin-β-deficient Nerves during Regeneration—The delayed regeneration of meltrin-β-deficient nerves could be caused by a defect in development of the Schwann cell, including its proliferation, viability, and differentiation. For this reason, we compared Schwann cell viability and proliferation in wild type and meltrin-β-deficient sciatic nerves during regeneration. There was little apoptosis in the lesioned nerves of meltrin-β-deficient mice, as evidenced by similar numbers of cleaved caspase-3-positive apoptotic cells that were observed in the part distal to the lesion of wild type and meltrin-β-deficient nerves 4 days after nerve crush (data not shown). Bromodeoxyuridine incorporation into glial fibrillary acidic protein-positive immature Schwann cells was similar in the nerves from both genotypes at 7 days after nerve crush (bromodeoxyuridine incorporation in each microscopic field of 100 × 100 μm^2: wild type, 13.7 ± 1.0; mutant, 13.0 ± 2; $n = 4$). Similar numbers of GFAP-positive cells were found in wild type and meltrin-β-deficient nerves (data not shown). Thus, the viability and

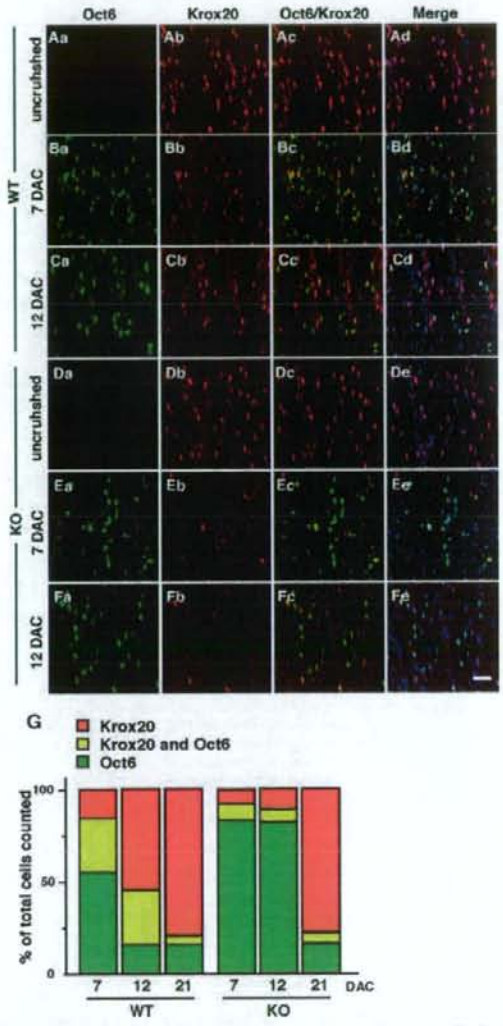

FIGURE 4. **Delayed generation of Krox-20-positive Schwann cells during regeneration in meltrin-β-deficient nerves.** *A–F*, longitudinal sections of uninjured or injured nerves at 7 (*B* and *E*) and 12 (*C* and *F*) DAC were prepared from wild type (*WT*) and mutant (*KO*) mice. Each section was immunostained with antibodies against transcription factors, Oct-6 (*green*) and Krox-20 (*red*). The nuclei were stained with 4′,6-diamidino-2-phenylindole (shown in merged profiles). *Scale bar*, 100 μm. *G*, the percentage of cells expressing only Krox-20 (*red*), Krox-20 and Oct-6 (*yellow green*), and only Oct-6 (*green*) in the cells expressing Krox-20 and/or Oct-6 at 7, 12, and 21 DAC. Note that the progression of Schwann cell differentiation from Oct-6$^+$Krox-20$^-$ to Oct-6$^+$Krox-20$^+$ and then to Oct-6$^-$Krox-20$^+$-myelinating cells are delayed in the mutant nerves.

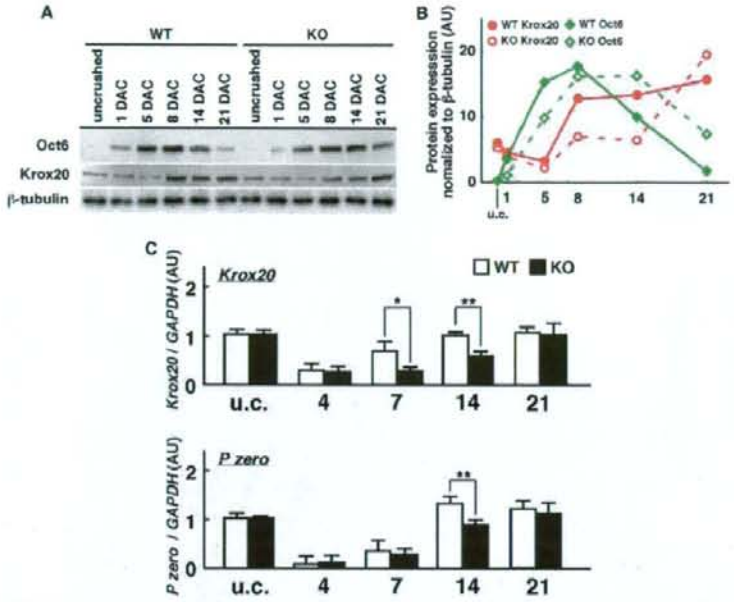

FIGURE 5. **Delayed activation of Krox-20 during regeneration in meltrin-β-deficient nerves.** *A*, Western blots of cell lysates prepared from the lesioned nerves at the indicated days after nerve crush using antibodies against Oct-6 (*upper panel*) and Krox-20 (*middle panel*). Twenty micrograms of proteins were contained in each lane. A representative experiment is shown here. The expression of β-tubulin protein was used as a control for protein loading (*bottom panel*). *B*, expression of Krox-20 (*red*) and that of Oct-6 (*green*) in the lesioned nerves of wild type (*solid lines*) and mutant (*dotted lines*) mice after nerve crush were quantified on the basis of the amount of β-tubulin. Note that lags of several days occurred in the activation of Krox-20 and down-regulation of Oct-6 in mutant nerves. *AU*, arbitrary units; u.c., uncrushed. *C*, levels of Krox-20 and P0 transcripts in the lesioned nerves specified days after the crush. Quantitative RT-PCR products of Krox-20 and P0 mRNA were normalized with those of glyceraldehyde-3-phosphate dehydrogenase (*GAPDH*) mRNA. The mean ± S.E. from three wild type mice and four mutant mice are represented (*, $p < 0.01$; **, $p < 0.05$, Fischer's PLSD test.).

proliferation of immature Schwann cells in wild type and meltrin-β-deficient nerves during regeneration were similar to each other.

We then examined whether meltrin-β-deficient mice have any defects in Schwann cell differentiation during regeneration. As shown above, morphological analyses revealed less myelinated axons and much thinner myelin sheaths of meltrin-β-deficient nerves than those of wild type nerves at early stages of regeneration. It was, therefore, most likely that the progression of Schwann cell differentiation during regeneration was affected in meltrin-β-deficient nerves. This observation led us to investigate expression of two different transcription factors, Oct-6 and Krox-20, both of which are pivotal regulators of the transcriptional program of myelination (2–4). Oct-6 marks demyelinating, promyelin Schwann cells, whereas Krox-20 is activated in Schwann cells in the process of myelination. Investigation of Krox-20 expression is especially important because it plays essential roles in myelination and transcriptional activation of the myelin protein genes such as myelin basic protein and protein zero (P0) genes (29, 30). Immunostaining of wild type and meltrin-β-deficient nerves revealed that Oct-6 expression was markedly induced in both genotypes 7 days after nerve crush (Fig. 4). Wild type and mutant nerves, however, contained Schwann cells of different stages; wild type nerves contained a considerable number of Oct-6$^+$Krox-20$^+$ Schwann cells in addition to Oct-6$^+$Krox-20$^-$ cells, whereas the majority of Schwann cells in mutant nerves were Oct-6$^+$Krox-20$^-$ (Fig. 4, *B*, *E*, and *G*, and supplemental data). The result indicated that activation of Krox-20 initiates in promyelin Schwann cells in regenerating nerves of wild type mice but not in those of the mutant mice at 7 DAC. Twelve days after the crush, a prominent increase in the number of Oct-6$^-$Krox-20$^+$-myelinating cells was observed in wild type nerves, whereas most Schwann cells in mutant nerves were Oct-6$^+$Krox-20$^-$ and Oct-6$^+$Krox-20$^+$, still devoid of Oct-6$^-$Krox-20$^+$-myelinating cells (Fig. 4, *C*, *F*, and *G*, and supplemental data; percentage of Oct-6$^-$Krox-20$^+$ cells in each microscopic: wild type, 52.8 ± 6.1; mutant, 11.0 ± 1.6; $n = 3$). Subsequently, a prominent activation of Krox-20 also occurred in the mutant nerves between 2 and 3 weeks after the injury that resulted in increased Oct-6$^-$Krox-20$^+$-myelinating cells in these mice (Fig. 4*G*). These results showed that the progression of Schwann cell differentiation from Oct-6$^+$Krox-20$^-$ to Oct-6$^+$Krox-20$^+$ and then to Oct-6$^-$Krox-20$^+$-myelinating cells is delayed in the meltrin-β-deficient nerves.

To quantify the levels of Oct-6 and Krox-20 during the nerve regeneration, we collected sciatic nerves of wild type and mutant mice at various days after crush injury and examined the expression of both of these transcription factors by immunoblot analysis (Fig. 5*A*). We found that the transition of Schwann cells from Oct-6-dominant to Krox-20-dominant stages in meltrin-β-deficient mice lagged about 1 week behind that in wild type mice (Fig. 5*B*). Analyses with quantitative RT-PCR revealed that the delayed activation of Krox-20 resulted in retarded transcriptional activation of the P0 gene, one of the major myelin components of the PNS, in regenerating nerves of meltrin-β-deficient mice (Fig. 5*C*). Together with morphological analyses, these results indicate that meltrin-β participates in the progression of Schwann cell differentiation, mainly in the transition from Oct-6-dominant promyelin to Krox-20-dominant myelinating stages.

Decreased Activation of PI3K—Akt signals in regenerating meltrin-β-deficient nerves. Schwann cell development, including proliferation and differentiation, is regulated by various growth factors, such as NRG and insulin-like growth factor I (IGF-I). Receptors for these growth factors are classified as receptor-tyrosine kinases, which transmit intracellular signals mainly through the Erk and PI3K pathways (6). To compare

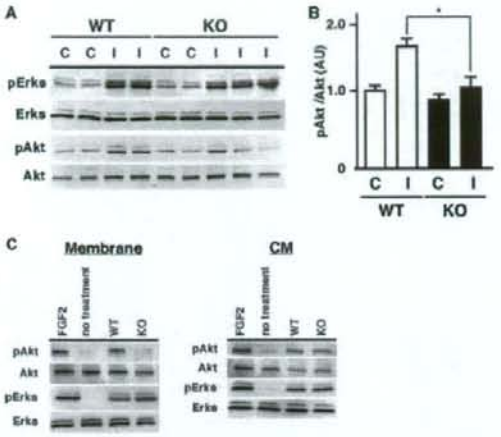

FIGURE 6. **Decreased activation of Akt, but not Erks, during regeneration in meltrin-β-deficient nerves.** *A*, lysates were prepared from the contralateral (*C*) and ipsilateral (*I*) sides of the sciatic nerves at 7 days after crush injury and analyzed by immunoblotting for phospho-Akt (*pAkt*), total Akt, phospho-Erk (*pErks*), and total Erks. *WT*, wild type; *KO*, knock out. *B*, quantification of phosphorylated Akt in the wild type or mutant nerves 7 days after the crush injury. The *bar graph* indicates the ratio of phospho-Akt to total Akt. The means ± S.E. from six wild type and five mutant mice are represented (*, $p < 0.05$, Fischer's PLSD test.). *C*, membranes or conditioned media (*CM*) prepared from wild type and mutant neuron cultures were plated onto Schwann cell cultures, and after 20 min lysates were prepared, blotted, and probed for phospho-Akt, total Akt, phospho-Erk, and total Erks as shown.

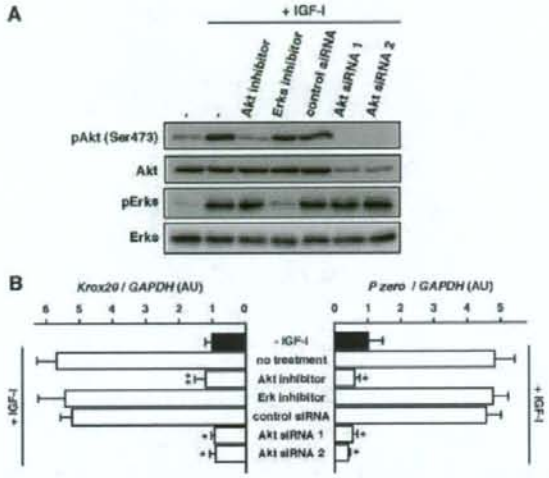

FIGURE 7. **Knockdown or pharmacological inhibition of Akt abrogates expression of Krox-20 and P0 genes in Schwann cells.** *A*, Western blots of cell lysates prepared from cultured primary Schwann cells after treatment of inhibitors or transfection of siRNA is shown. Twenty micrograms of proteins were contained in each lane. Note that the activation of Akt induced by exposure to IGF-I was inhibited by Akt inhibitor IV (1 μM) but not by Erk inhibitor, U0126 (5 μM). The expression of Akt protein was inhibited by transfection of Akt targeting siRNAs. *B*, effects of pharmacological inhibitors and siRNAs on the transcriptional activation of Krox-20 and P0 genes in Schwann cells stimulated with IGF-I. Quantitative RT-PCR products of Krox-20 and P0 mRNA were normalized with those of glyceraldehyde-3-phosphate dehydrogenase (*GAPDH*) mRNA. Note that induction of Krox-20 and P0 transcripts by 2 days of exposure to IGF-I was blocked by Akt inhibitor IV (1 μM) but not by Erk inhibitor, U0126 (5 μM). The activation of Krox-20 and P0 transcripts was also inhibited in the Schwann cells transfected with Akt-specific siRNA. The means ± S.E. from three independent experiments are represented (*, $p < 0.05$; **, $p < 0.01$, Fischer's PLSD test). *AU*, arbitrary units.

intracellular signals mediated by Erk and PI3K-Akt pathways in wild type and meltrin-β-deficient mice, sciatic nerves were isolated at 7 days after the crush injury, and the phosphorylation of Erk and Akt was examined by immunoblotting and densitometric analysis (Fig. 6, *A* and *B*). In wild type and meltrin-β-deficient regenerating nerves, a similar level of phosphorylation of Erks was observed. In contrast, the level of phosphorylation of Akt was significantly reduced in meltrin-β-deficient nerves compared with wild type nerves.

Recent studies indicate that signals mediated by PI3K-Akt are crucial for initiation of myelination and that the effects of growth factors on the progression of Schwann cell differentiation are primarily dependent on the balance between the Erk and PI3K-Akt activation (7, 8). We examined whether the pharmacological inhibition or the targeted knockdown of Akt with siRNA against it in Schwann cells affects activation of Krox-20 and P0. As shown in Fig. 7, activation of Krox-20 and P0 transcripts by the treatment of IGF-I were prominently reduced by a pharmacological inhibition of Akt activation or a targeted knockdown of Akt expression but not by an inhibition of Erk activation, suggesting that Akt and its signaling pathway mediates Krox-20 activation and the myelination program that requires Krox-20.

Contact-dependent, juxtacrine signaling from axons is required for the activation of PI3K-Akt pathway in Schwann cells that initiate myelination (31, 32). To explore whether the impaired contact-dependent signaling in meltrin-β-deficient nerves causes the decreased phosphorylation of Akt in Schwann cells, we plated membrane fractions prepared from wild type and meltrin-β-deficient neuron cultures onto Schwann cells for 20 min and then measured the levels of phospho-Akt and phospho-Erk (Fig. 6C). As a result, the activation of PI3K-Akt pathway was consistently reduced with the meltrin-β-deficient membrane fraction, whereas it activated Erk similarly to the wild type membrane fraction. No significant difference was found between the effects of conditioned media prepared from wild type and meltrin-β-deficient neuron culture. The effects of conditioned medium and membrane preparation of primary nerve culture should represent the involvement of paracrine and juxtacrine signaling mechanisms, respectively. These results suggest that meltrin-β-deficient nerves are defective in presenting contact-dependent signaling from axons to Schwann cells that is required for the activation of PI3K-Akt pathway, the up-regulation of Krox-20, and the onset of myelination during regeneration.

Delayed Functional Recovery after Nerve Crush in Meltrin-β-deficient Mice—Finally, we examined whether the retardation of remyelination after nerve crush affected functional recovery of the injured nerves in meltrin-β-deficient mice. Two types of behavior tests, toe-spreading and grip strength tests (25, 26, 33), were performed (Fig. 8). Rodents spread the toes of their hind feet on contact with a solid surface, which is a reflex that requires sensory innervation (25, 26, 33). The ability to spread the toes, therefore, is diminished after the crush injury and returns to normal as sensory axon reinnervation recovers. In

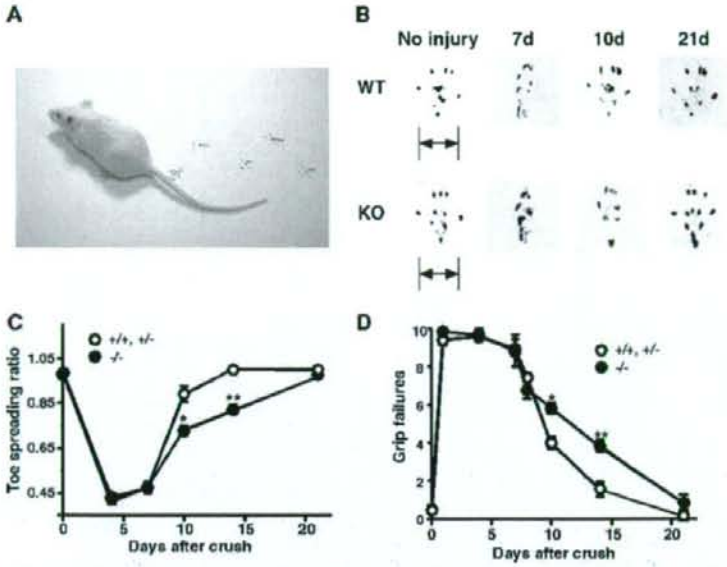

FIGURE 8. **Sciatic functional recovery after crush injury is delayed in meltrin-β-deficient mice.** *A*, toe-spreading test of mice after sciatic nerve injury (see "Materials and Methods"). *B*, footprints of wild type (*WT*) and meltrin-β-deficient (*KO*) mice at the specified days after sciatic nerve injury. In the first column the toe-spread distance is indicated. *C*, recovery of toe spread after sciatic nerve crush. Retarded recovery is found in mutant mice. *D*, grip failures after sciatic nerve crush. All data are represented as means ± S.E. from five wild type mice and seven mutant mice. *, $p < 0.05$; **, $p < 0.005$ compared with wild type, Fischer's PLSD test.

the toe-spreading measurement, wild type mice exhibited significant declines in the index of toe spreading immediately after sciatic injury and then recovered progressively from 7 to 21 days post-injury. In meltrin-β-deficient mice, the index began to recover at day 7 similarly to that in wild type mice. However, the recovery rate of the index was significantly slower, with a lag period of several days behind that of wild type mice. On the other hand, when injured in the hind limb, mice frequently fail to grip gridd wire with the injured leg until grip strength recovers. In this grip strength test, the number of failed trials until each mouse succeeds in gripping the grids with its injured leg is measured (25). The grip strength recovery of meltrin-β-deficient mice lagged significantly behind that of wild type mice 1 to 2 weeks after injury but by 3 weeks after injury had attained a level comparable with that of wild type mice. These results indicated that the sciatic functional recovery is delayed in meltrin-β-deficient mice.

DISCUSSION

Using the sciatic nerve crush as a well established paradigm of regenerating lesions, we showed here that meltrin-β (ADAM19) participates in efficient progression of nerve regeneration. Tissue regeneration recapitulates developmental programs in general, and PNS regeneration is preceded by Wallerian degeneration (27). This process involves degradation of injured axons and myelin sheath and removal of phagocytic debris by macrophages. Several proteases are involved in these early events. Membrane type-5 matrix metalloproteinase, for example, degrades the core proteins of chondroitin sulfate proteoglycans, which are abundant in neuronal tissues and inhibitory to axonal outgrowth (34, 35). In contrast, the early events after the crush injury including Wallerian degeneration and axon elongation were not affected in meltrin-β-deficient mice (Figs. 2 and 3). Instead, meltrin-β played roles in Schwann cell differentiation. Immature Schwann cells differentiate to myelinating cells via a promyelin stage during which Schwann cells establish a one-to-one relationship with axons. The Schwann cells are arrested at the promyelin stage in Krox-20 hypomorphic mice ($Egr2^{1.o/1.o}$) and in mice deficient in Nab proteins that associate with Krox-20 (36, 37); expression of Oct-6 remains high in both of these mice. This indicates that Schwann cells pass through an Oct-6$^+$ transitional stage before entering the Krox-20$^+$ myelinating stage and that functional Krox-20 is required for myelination (38, 39). Analyses of meltrin-β-deficient nerves revealed that meltrin-β is involved in the efficient progression from the Oct-6$^+$ to the Krox-20$^+$ stage. Thus, delayed transition of Schwann cells from the Oct-6$^+$ promyelin to Krox-20$^+$-myelinating stage in meltrin-β-deficient nerves could be caused by inefficient activation of Krox-20 in nerve regeneration.

Previous studies showed that the PI3K-Akt pathway is crucial for initiation of myelination, whereas those of Erks have an opposing effect on Schwann cells; that is, cell proliferation and/or the inhibition of myelination (7, 8). Moreover, contact-dependent, juxtacrine signaling from axons mediates the activation of PI3K-Akt pathway, but not the activation of Erk pathway, in Schwann cells that initiate myelination (31, 32). In this study we showed that activation of Akt is required for transcriptional activation of Krox-20 in Schwann cells (Fig. 7). Thus, activation of Krox-20 is dependent on activation of Akt, and juxtacrine mechanisms mediate the activation of Akt pathway in Schwann cells during myelination. We, therefore, asked whether the inability of meltrin-β-deficient nerves to activate Krox-20 in Schwann cells could be due to an impaired activation of Akt and inefficient juxtacrine signaling critical for the activation of Akt in the nerves. As a result, a significant decrease in Akt activation was observed in meltrin-β-deficient nerves during regeneration. Moreover, activation of Akt in Schwann cells with the membrane fraction prepared from meltrin-β-deficient nerves was less efficient than that with the membrane fraction prepared from wild type nerves (Fig. 6*C*). The effect of membrane preparation of primary nerve culture should represent the involvement of juxtacrine signaling mechanisms. These data suggest that meltrin-β is involved in the activation of juxtacrine signaling from the nerves that stimulates the Akt pathway in Schwann cells.

Genetic evidence suggests that the axon-derived juxtacrine signal that activates a PI3K-Akt pathway for myelination is dependent on NRG1 type III, an isoform of NRG1 containing two membrane-spanning regions (31, 32), and BACE1, a β-secretase that is involved in the production of β-amyloid (40). BACE1 is responsible for the ectodomain shedding of NRG1 type III and activates the Akt pathway for the axon myelination (41). The mechanism of how NRG1 type III activates Akt has not been elucidated.

In contrast to BACE1, meltrin-β does not enhance the cleavage of NRG1 type III but enhances the cleavage of NRG1 type I (16, 17). Although the cleavage of a single site in the ectodomain of NRG1 type III results in the generation of a growth factor as a form of type I membrane protein (42), the ectodomain shedding of NRG1 type I, an isoform sharing an ErbB ligand domain with NRG1 type III but containing a single membrane-spanning region, generates soluble ligands for ErbB that activates Erk. The soluble NRG1 not only plays a role in differentiation of immature Schwann cell precursors to the promyelin stage but also transforms myelinated Schwann cells into promyelin cells through the reverse activation of Oct-6 in the myelinated cells (28, 43). Thus, the progression of Schwann cell differentiation from promyelin to myelinating stages accompanies the transition of ErbB signaling from NRG1 type I to type III-dependent or from paracrine to juxtacrine mode. In contrast to tumor necrosis factor-α-converting enzyme, which is essential for phorbol ester-enhanced ectodomain shedding of NRG1 type I, meltrin-β is involved in its constitutive ectodomain shedding, leading to the depletion of soluble NRG1 to be secreted (18). Based on these genetic and biochemical analyses, we hypothesize that depletion of NRG1 type I with meltrin-β is required for the activation of NRG1 type III-dependent signaling, which proceeds Schwann cell differentiation from Erk/Oct-6 promyelin to Akt/Krox20-dependent myelination stage. Not only delayed activation of Krox-20 but also prolonged activation of Oct-6 in meltrin-β-deficient nerves during regeneration (Fig. 5*B*) support this hypothesis. Alternatively, meltrin-β may be involved in peri-membranous events that cooperate with NRG1 type III signaling during myelination. Domains of meltrin-β other than the protease domain may also play some roles in the myelination pathway. Further studies will elucidate the regulatory mechanisms by which meltrin-β activates Akt signaling required for myelination.

In summary, this study showed that meltrin-β is involved in Schwann cell differentiation and myelination of regenerating axons after crush injury. The impairment of remyelination in meltrin-β-deficient nerves was accomplished at a later time point after the crush. Roles of meltrin-β in nerve regeneration may be compensated by other proteases such as tumor necrosis factor-α-converting enzyme. Two types of behavior tests were used to confirm delayed functional recovery of PNS after the nerve crush in meltrin-β-deficient mice. These tests evaluate crucial aspects of locomotion involving recovery of hindlimb sensory and motor function (25, 26, 33). The functions of ADAM proteins including meltrin-β as modulators of growth factor signaling and cell-cell interactions in neural development and regeneration provide novel avenues for understanding development and maintenance of neural tissues.

Acknowledgments—We thank M. Fujioka of Kyoto University for technical support in the preparation of sciatic nerve semi-thin sections and F. Saitoh of National Center for Neurology and Psychiatry for technical suggestions. We also thank T. Kurisaki for critical comments to this manuscript.

REFERENCES

1. Jessen, K. R., and Mirsky, R. (2005) *Nat. Rev. Neurosci.* **6,** 671–682
2. Topilko, P., Schneider-Maunoury, S., Levi, G., Baron-Van Evercooren, A., Chennoufi, A. B., Seitanidou, T., Babinet, C., and Charnay, P. (1994) *Nature* **371,** 796–799
3. Bermingham, J. R., Jr., Scherer, S. S., O'Connell, S., Arroyo, E., Kalla, K. A., Powell, F. L., and Rosenfeld, M. G. (1996) *Genes Dev.* **10,** 1751–1762
4. Jaegle, M., Mandemakers, W., Broos, L., Zwart, R., Karis, A., Visser, P., Grosveld, F., and Meijer, D. (1996) *Science* **273,** 507–510
5. Garratt, A. N., Britsch, S., and Birchmeier, C. (2000) *BioEssays* **22,** 987–996
6. Hunter, T. (1997) *Cell* **88,** 333–346
7. Ogata, T., Iijima, S., Hoshikawa, S., Miura, T., Yamamoto, S., Oda, H., Nakamura, K., and Tanaka, S. (2004) *J. Neurosci.* **24,** 6724–6732
8. Harrisingh, M. C., Perez-Nadales, E., Parkinson, D. B., Malcolm, D. S., Mudge, A. W., and Lloyd, A. C. (2004) *EMBO J.* **23,** 3061–3071
9. Janes, P. W., Saha, N., Barton, W. A., Kolev, M. V., Wimmer-Kleikamp, S. H., Nievergall, E., Blobel, C. P., Himanen, J. P., Lackmann, M., and Nikolov, D. B. (2005) *Cell* **123,** 291–304
10. Qi, H., Rand, M. D., Wu, X., Sestan, N., Wang, W., Rakic, P., Xu, T., and Artavanis-Tsakonas, S. (1999) *Science* **283,** 91–94
11. Reiss, K., Maretzky, T., Ludwig, A., Tousseyn, T., de Strooper, B., Hartmann, D., and Saftig, P. (2005) *EMBO J.* **24,** 742–752
12. Blobel, C. P. (2005) *Nat. Rev. Mol. Cell Biol.* **6,** 32–43
13. Yagami-Hiromasa, T., Sato, T., Kurisaki, T., Kamijo, K., Nabeshima, Y., and Fujisawa-Sehara, A. (1995) *Nature* **377,** 652–656
14. Kurisaki, T., Masuda, A., Osumi, N., Nabeshima, Y., and Fujisawa-Sehara, A. (1998) *Mech. Dev.* **73,** 211–215
15. Inoue, D., Reid, M., Lum, L., Kratzschmar, J., Weskamp, G., Myung, Y. M., Baron, R., and Blobel, C. P. (1998) *J. Biol. Chem.* **273,** 4180–4187
16. Shirakabe, K., Wakatsuki, S., Kurisaki, T., and Fujisawa-Sehara, A. (2001) *J. Biol. Chem.* **276,** 9352–9358
17. Wakatsuki, S., Kurisaki, T., and Sehara-Fujisawa, A. (2004) *J. Neurochem.* **89,** 119–123
18. Yokozeki, T., Wakatsuki, S., Hatsuzawa, K., Black, R. A., Wada, I., and Sehara-Fujisawa, A. (2007) *Genes Cells* **12,** 329–343
19. Zhou, H. M., Weskamp, G., Chesneau, V., Sahin, U., Vortkamp, A., Horiuchi, K., Chiusaroli, R., Hahn, R., Wilkes, D., Fisher, P., Baron, R., Manova, K., Basson, C. T., Hempstead, B., and Blobel, C. P. (2004) *Mol. Cell. Biol.* **24,** 96–104
20. Takeda, S., Igarashi, T., Mori, H., and Araki, S. (2006) *EMBO J.* **25,** 2388–2396
21. Komatsu, K., Wakatsuki, S., Yamada, S., Yamamura, K., Miyazaki, J., and Sehara-Fujisawa, A. (2007) *Dev. Biol.* **303,** 82–92
22. Kurohara, K., Komatsu, K., Kurisaki, T., Masuda, A., Irie, N., Asano, M., Sudo, K., Nabeshima, Y., Iwakura, Y., and Sehara-Fujisawa, A. (2004) *Dev. Biol.* **267,** 14–28
23. Maurel, P., and Salzer, J. L. (2000) *J. Neurosci.* **20,** 4635–4645
24. Contreras, P. C., Steffler, C., Yu, E., Callison, K., Stong, D., and Vaught, J. L. (1995) *J. Pharmacol. Exp. Ther.* **274,** 1443–1449
25. Kim, J. E., Bonilla, I. E., Qiu, D., and Strittmatter, S. M. (2003) *Mol. Cell. Neurosci.* **23,** 451–459
26. Pot, C., Simonen, M., Weinmann, O., Schnell, L., Christ, F., Stoeckle, S., Berger, P., Rulicke, T., Suter, U., and Schwab, M. E. (2002) *J. Cell Biol.* **159,** 29–35
27. Waller, A. (1851) *Edinburgh Med. Surg. J.* **76,** 369–376
28. Chen, Z. L., and Strickland, S. (2003) *J. Cell Biol.* **163,** 889–899

29. Yin, X., Kidd, G. J., Wrabetz, L., Feltri, M. L., Messing, A., and Trapp, B. D. (2000) *J. Cell Biol.* **148,** 1009–1020
30. Garbay, B., Heape, A. M., Sargueil, F., and Cassagne, C. (2000) *Prog. Neurobiol.* **61,** 267–304
31. Taveggia, C., Zanazzi, G., Petrylak, A., Yano, H., Rosenbluth, J., Einheber, S., Xu, X., Esper, R. M., Loeb, J. A., Shrager, P., Chao, M. V., Falls, D. L., Role, L., and Salzer, J. L. (2005) *Neuron* **47,** 681–694
32. Salzer, J. L. (2008) *J. Cell Biol.* **181,** 575–577
33. Holmes, F. E., Bacon, A., Pope, R. J., Vanderplank, P. A., Kerr, N. C., Sukumaran, M., Pachnis, V., and Wynick, D. (2003) *Proc. Natl. Acad. Sci. U. S. A.* **100,** 6180–6185
34. Zuo, J., Ferguson, T. A., Hernandez, Y. J., Stetler-Stevenson, W. G., and Muir, D. (1998) *J. Neurosci.* **18,** 5203–5211
35. Jones, L. L., Yamaguchi, Y., Stallcup, W. B., and Tuszynski, M. H. (2002) *J. Neurosci.* **22,** 2792–2803
36. Le, N., Nagarajan, R., Wang, J. Y., Svaren, J., LaPash, C., Araki, T., Schmidt, R. E., and Milbrandt, J. (2005) *Nat. Neurosci.* **8,** 932–940
37. Le, N., Nagarajan, R., Wang, J. Y., Araki, T., Schmidt, R. E., and Milbrandt, J. (2005) *Proc. Natl. Acad. Sci. U. S. A.* **102,** 2596–2601
38. Nagarajan, R., Svaren, J., Le, N., Araki, T., Watson, M., and Milbrandt, J. (2001) *Neuron* **30,** 355–368
39. Parkinson, D. B., Bhaskaran, A., Arthur-Farraj, P., Noon, L. A., Woodhoo, A., Lloyd, A. C., Feltri, M. L., Wrabetz, L., Behrens, A., Mirsky, R., and Jessen, K. R. (2008) *J. Cell Biol.* **181,** 625–637
40. LaFerla, F. M., Green, K. N., and Oddo, S. (2007) *Nat. Rev. Neurosci.* **8,** 499–509
41. Hu, X., Hicks, C. W., He, W., Wong, P., Macklin, W. B., Trapp, B. D., and Yan, R. (2006) *Nat. Neurosci.* **9,** 1520–1525
42. Nave, K. A., and Salzer, J. L. (2006) *Curr. Opin. Neurobiol.* **16,** 492–500
43. Zanazzi, G., Einheber, S., Westreich, R., Hannocks, M. J., Bedell-Hogan, D., Marchionni, M. A., and Salzer, J. L. (2001) *J. Cell Biol.* **152,** 1289–1299

Human Molecular Genetics, 2009, Vol. 18, No. 5 **942–955**
doi:10.1093/hmg/ddn422
Advance Access published on December 16, 2008

Mutant SOD1 impairs axonal transport of choline acetyltransferase and acetylcholine release by sequestering KAP3

Minako Tateno[1], Shinsuke Kato[2], Takashi Sakurai[3,†], Nobuyuki Nukina[3], Ryosuke Takahashi[4] and Toshiyuki Araki[1,*]

[1]Department of Peripheral Nervous System Research, National Institute of Neuroscience, National Center of Neurology and Psychiatry, 4-1-1 Ogawa-Higashi, Kodaira, Tokyo 187-8502, Japan, [2]Department of Neuropathology, Institute of Neurological Sciences, Tottori University Faculty of Medicine, 36-1 Nishi-cho, Yonago, Tottori 683-8504, Japan, [3]Laboratory for Structural Neuropathology, RIKEN Brain Science Institute, 2-1 Hirosawa, Wako, Saitama 351-0198, Japan and [4]Department of Neurology, Kyoto University Graduate School of Medicine, 54 Kawahara-cho, Shogoin, Sakyo-ku, Kyoto 606-8507, Japan

Received September 11, 2008; Revised and Accepted December 9, 2008

Mutations in the *superoxide dismutase 1* (*sod1*) gene cause familial amyotrophic lateral sclerosis (FALS), likely due to the toxic properties of misfolded mutant SOD1 protein. Here we demonstrated that, starting from the pre-onset stage of FALS, misfolded SOD1 species associates specifically with kinesin-associated protein 3 (KAP3) in the ventral white matter of *SOD1*^{G93A}-transgenic mouse spinal cord. KAP3 is a kinesin-2 subunit responsible for binding to cargos including choline acetyltransferase (ChAT). Motor axons in *SOD1*^{G93A}-Tg mice also showed a reduction in ChAT transport from the pre-onset stage. By employing a novel FALS modeling system using NG108-15 cells, we showed that microtubule-dependent release of acetylcholine was significantly impaired by misfolded SOD1 species. Furthermore, such impairment was able to be normalized by KAP3 overexpression. KAP3 was incorporated into SOD1 aggregates in human FALS cases as well. These results suggest that KAP3 sequestration by misfolded SOD1 species and the resultant inhibition of ChAT transport play a role in the dysfunction of ALS.

INTRODUCTION

Amyotrophic lateral sclerosis (ALS) is a fatal, progressive neurodegenerative disease characterized by motor neuron cell death in the brain and spinal cord accompanied by rapid loss of muscle control and eventually complete paralysis (1,2). The vast majority of ALS cases are of a sporadic nature, while ~10% are familial (FALS). Although the cause of sporadic ALS remains unclear, 15–20% of FALS patients have point mutations in cytosolic Cu^{2+}/Zn^{2+} superoxide dismutase (SOD1). SOD1 is an antioxidant enzyme ubiquitously expressed in the cytosol, which converts the superoxide anion radical to hydrogen peroxide. More than 115 disease-causing mutations, affecting all regions of the SOD1 gene product, have been identified.

Previous studies using transgenic animal models expressing mutated human SOD1 have shown that the disease is not caused by a loss of its dismutase activity, but by the gain of toxic properties (1). Many mutant SOD1 proteins tend to become easily misfolded and form aggregates, especially under oxidative stress (3,4). Intracellular aggregates containing SOD1 were specifically detected in affected regions of both patients and animal models possessing *sod1* mutations (5–7). In spinal cords of mutant SOD1-Tg mice, misfolded intermediates of mutant SOD1 proteins, which showed a decrease in solubility and increase in size, were found prior to disease onset (8,9). These results suggest that misfolded molecules containing mutant SOD1 may contribute to motor neuron-specific damage in ALS.

*To whom correspondence should be addressed. +81 423461716; Fax: +81 423461746; Email: taraki@ncnp.go.jp
†Present address: Department of Pharmacology, Juntendo University School of Medicine, 2-1-1 Hongo, Bunkyo-ku, Tokyo, 113-8421 Japan.

Axonal transport is required for a variety of neural functions including neurotransmitter synthesis, release and recycling (10). Motor neurons often have long axons that can be more than a meter in length in humans. For this reason, orderly function of the axonal transport mechanism should be particularly important in maintaining the structure and signal transmission at the terminals of motor axons. The transport process is carried out by two major families of motor proteins, i.e. kinesin super family for anterograde transport and the cytoplasimic dynein for retrograde transport (11). Defects in axonal transport have been reported as an early sign of motor neuron diseases including ALS (12). In mutant SOD1-Tg mice, anterograde transport of neurofilaments and tubulin is partially impaired long before disease onset, presumably due to an inhibition of certain transport systems (13,14). With respect to retrograde transport, mutations in the dynein heavy chain result in motor-selective dysfunction in mice (15). Moreover, mutation in $p150^{Glued}$, a subunit of dynactin (dynein activator), was identified in a family that developed a lower motor neuron-specific disease (16). These results strongly suggest a link between the integrity of the axonal transport mechanism with the function and survival of motor neurons.

We previously studied the intracellular localization of misfolded SOD1 species by subcellular fractionation of spinal cords from *SOD1*^{G93A}-Tg mice and found a significant accumulation of misfolded SOD1 species within the axon-enriched fraction at disease onset (17). From this result, together with previous reports, we hypothesized that misfolded SOD1 species may bind to proteins required for axonal transport and thereby inhibit normal function of the motor proteins. To prove this hypothesis, we screened axonal transport-related molecules in search for proteins that associate specifically to the misfolded SOD1 species and identified KAP3 as a misfolded SOD1-interacting protein. KAP3 is a component of the kinesin-2 motor complex mediating an axonal transport of choline acetyltransferase (ChAT) in *Drosophila* (18,19). By using an *in vitro* FALS modeling system that we developed, we showed that misfolded SOD1 inhibits axonal transport-dependent release of acetylcholine (ACh). Moreover, such impairment of ACh release could be rescued by the KAP3 overexpression. This evidence strongly suggests that the sequestering of KAP3 and the resultant inhibition of ChAT transport is a novel toxic property of mutant SOD1 proteins that inevitably leads to motor neuron-specific dysfunction.

RESULTS

Misfolded SOD1 species is accumulated in ventral white matter of spinal cords in *SOD1*^{G93A}-Tg mice prior to disease onset

We previously showed by using subcellular fractionation analysis that a considerable amount of misfolded SOD1 species is located in a fraction enriched in nucleus and certain kinds of cytoskeletal proteins (i.e. glial fibrilary acidic protein and neurofilament) in *SOD1*^{G93A}-Tg mice spinal cord prior to appearance of characteristic motor symptoms of ALS (17). To analyze more detailed subcellular localization of misfolded SOD1 in spinal motor neurons of *SOD1*^{G93A}-Tg mice, we divided the spinal cord into four subsegments by laser-assisted microdissection (LMD) (summarized in Fig. 1A) and used the lysate from each segment to detect SOD1 by immunoblot analysis. Since we observed that the *SOD1*^{G93A}-Tg mice we used in this study experienced disease onset around the age of 8 months (246.5 ± 5.8 days) and died around 9.5 months (288.5 ± 7.1 days, mean $\pm$ SEM, $n = 14$), we chose to collect samples from mice of 4, 7, 8 and 9 months of age. As expected, the majority of misfolded SOD1 species (high molecular-weight bands/smears immunoreactive for SOD1) was located in the ventral gray matter at 7 months of age, which is 1 month prior to disease onset (Fig. 1B and C). At this age, we also found that a significant amount of misfolded SOD1 species was located in ventral white matter, suggesting that misfolded SOD1 species are localized in motor neuron cell bodies and their axons. We further divided the ventral white matter segment into three subsegments and confirmed a localization of misfolded SOD1 species to a motor axon-enriched segment indicated by ChAT expression (Supplementary Material, Fig. S1). Together, these results suggest that a significant amount of misfolded SOD1 species is located not only in motor neuron cell bodies, but also in motor axons of *SOD1*^{G93A}-Tg mice prior to disease onset.

Misfolded SOD1 species associates with KAP3, a kinesin-2 component

Previous reports strongly suggest that impairment of the axonal transport mechanism is linked to degeneration of motor neurons (12). Localization of misfolded SOD1 species in motor axons of *SOD1*^{G93A}-Tg mice suggests that misfolded SOD1 species may affect the function of proteins required for axonal transport. Anterograde and retrograde axonal transports are mediated by different protein complexes, which are composed of a large variety of proteins. The kinesin super family for anterograde transport, for instance, is divided into six families (kinesin-1, 2, 3, 4, 13 and 14) consisting of 45 members in human and mouse, and they associate with appropriate cargos via adaptor molecules in most cases (11). To gain more insight into the relationship between misfolded SOD1 and individual components of the molecular motor protein complex, we compared sedimentation of misfolded SOD1 in linear density gradient centrifugation with that of representative molecules that compose motor complexes in motor axon lysate. We asked whether any of these motor complex components co-migrate with misfolded SOD1. Homogenates were prepared from the ventral white matter of *SOD1*^{G93A}-Tg mice at 8 months of age (disease onset) and *SOD1*^{WT}-Tg mice expressing human wild-type *sod1* gene (non-symptomatic control) and subjected to linear Nycodenz density gradient centrifugation. SOD1 immunoreactive bands showing expected molecular weight (representing normally folded SOD1) were observed in fractions nos 1–7 in mice of both genotypes. Misfolded SOD1 species, on the other hand, were found in fractions around no. 16 only in *SOD1*^{G93A}-Tg mice. We then examined migration profiles of 17 major components of the molecular motors from five kinesin families excluding kinesin-4 which is mostly expressed in juvenile brain,

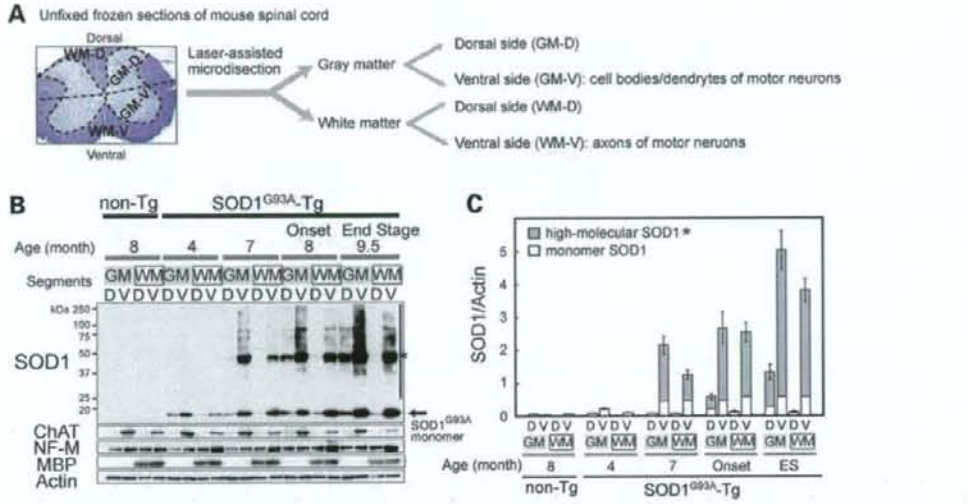

Figure 1. Misfolded SOD1 species were enriched in ventral white matter and ventral gray matter in spinal cord of *SOD1*^{G93A}-Tg mice prior to disease onset. (**A**) The procedure to divide and obtain subsegments of spinal cord is schematically shown. Unfixed frozen sections from L5 spinal cords were stained with 0.01% Toluidine blue and cut into four segments: dorsal white matter (WM-D), dorsal gray matter (GM-D), ventral white matter (WM-V) and ventral gray matter (GM-V) as indicated. (**B**) The presence of misfolded SOD1 species in the spinal cord subsegments obtained from 4, 7, 8 and 9.5 months old *SOD1*^{G93A}-Tg mice and 8 months old wild-type control (non-Tg) mice by immunoblot analysis is shown. Identity of the sample in each lane is indicated above the image. High molecular-weight bands/smears immunoreactive for SOD1 are the misfolded SOD1 species indicated by an asterisk. This misfolded SOD1 species appeared both in WM-V and GM-V of *SOD1*^{G93A}-Tg mice at 7 months. The same blot was analyzed for expression of ChAT (a motor neuron marker), neurofilament M (NF-M; a neuronal marker), MBP (a myelin marker) for controls. Actin served as a loading control. (**C**) The immunoreactivity of both monomeric (normally folded) and misfolded SOD1 that is shown in immunoblot analysis in (B) was quantified. The expression level of total SOD1 as well as monomeric and misfolded SOD1, in arbitrary units relative to actin expression is shown as a bar graph.

cytoplasmic dynein and dynactin. Among those molecules, KAP3, a subunit of the kinesin-2 motor complex, clearly co-migrated with misfolded SOD1 species around fraction no. 16 from *SOD1*^{G93A}-Tg mice (Fig. 2A, asterisks). In addition to KAP3, KIF3A and KIF3B, which are KAP3-binding partners, were weakly detected around fraction no. 16. We also observed p150^{Glued}, a dynactin subunit, co-migrated with misfolded SOD1 species. However, we did not proceed to a detailed analysis of this observation for now, because p50, another dynactin subunit (data not shown), or other dynein components such as Dynein intermediate chain (Dynein IC in Fig. 2A) did not co-migrate with misfolded SOD1 species. To confirm this association of KAP3 with misfolded SOD1, we performed immunoprecipitation analysis using the fraction nos 16 and 7. KAP3 was identified in anti-SOD1 immunoprecipitates obtained from fraction no. 16 containing misfolded SOD1 species but not in the fraction from no. 7 (Fig. 2B). In reciprocal immunoprecipitation, we found misfolded SOD1 in anti-KAP3 immunoprecipitates only in fraction no. 16. CRMP-2 (collapsin response mediator protein-2), a KAP3 counterpart for kinesin-1 motor complex, did not associate with misfolded SOD1. KAP3 seems to be associated with misfolded SOD1 species at least 2 months before disease onset, since the misfolded SOD1 species was detected in the immunoprecipitate with anti-KAP3 antibody from the extracts of 6-month-old *SOD1*^{G93A}-Tg spinal cords (Fig. 2C). Furthermore, we examined immunohistochemical localization of SOD1 and KAP3 on spinal cord sections of *SOD1*^{G93A}-Tg mice at 9 months of age (end stage). We found that protein aggregates in the remaining spinal motor neurons, immunoreactive for KAP3 were also positive for SOD1 (Fig. 2D, upper panel). The KAP3-positive aggregates also contained ubiquitin immunoreactivity, suggesting that the aggregates are cellular inclusion bodies (Fig. 2D, lower panel). These results suggest that misfolded SOD1 species specifically binds to KAP3 in motor axons of *SOD1*^{G93A}-Tg mice and that this association starts prior to the onset of motor symptoms.

Axonal transport of ChAT was significantly impaired in spinal motor neurons preceding disease onset in SOD1^{G93A}-Tg mice

Kinesin-2 is a ubiquitously and abundantly expressed molecular motor complex, which consists of KAP3 and KIF3A, together with either KIF3B or KIF3C (20). The motor domain consisting of KIF3A along with either KIF3B or KIF3C translocates along microtubules with hydrolyzing ATP, and KAP3 determines the specific cargo to be transported. Recent work using *Drosophila* ganglionic cells showed that kinesin-2 is involved in the transport of ChAT and ACh esterase (AChE) (18). Although both of the enzymes are essential for an efficient supply of ACh to the nerve terminals of spinal motor neurons, the amount of

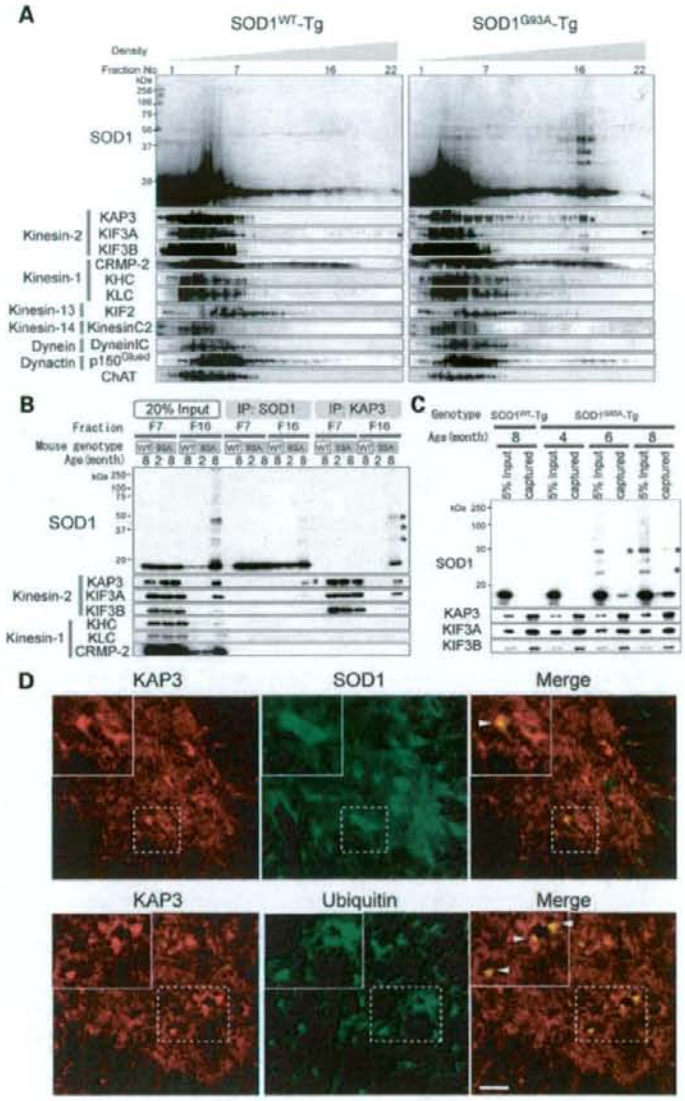

Figure 2. Misfolded SOD1 species in ventral white matter of spinal cords specifically associates with KAP3. (**A**) Fractions obtained from Nycodenz density gradient centrifugation of ventral white matter of 8-month-old *SOD1*^{WT}-Tg and *SOD1*^{G93A}-Tg spinal cords were analyzed for the presence of indicated proteins (SOD1 and individual components of kinesin and dynein motor complexes) by immunoblot analysis. Each lane (left to right) represents an aliquot collected from the top. Note that misfolded SOD1 species (indicated by asterisks) migrated around fraction no. 16 in *SOD1*^{G93A}-Tg spinal cords, where KAP3 co-migrated. (**B**) Immunoprecipitates of anti-SOD1 and KAP3 antibodies (indicated as 'IP:SOD1' or 'IP:KAP3') from Nycodenz density gradient centrifugation fractions 7 and 16 (F7, F16) of *SOD1*^{G93A}-Tg mouse spinal cords prepared above were analyzed for the presence of indicated proteins by immunoblot analysis. Also shown is an immunoblot of samples F7 and F16 (20% of the amount used for immunoprecipitation) examined for expression of the same set of proteins. Note that misfolded SOD1–KAP3 association was detected from F16 but not from F7. (**C**) Immunoprecipitates of anti-KAP3 antibody from whole spinal cord extracts of 4-, 6- and 8-month-old *SOD1*^{G93A}-Tg mice and 8-month-old *SOD1*^{WT}-Tg mice were analyzed for the presence of misfolded SOD1 by immunoblot. KIF3A and KIF3B, which are kinesin-2 components, served as controls for immunoprecipitation. Note that misfolded SOD1 species (asterisks) were captured by anti-KAP3 antibody in 6- and 8-month-old *SOD1*^{G93A}-Tg extracts. (**D**) Representative photographs of immunohistochemical co-localization of KAP3 and SOD1 (upper panel), and KAP3 and ubiquitin (lower panel) in a 9-month-old *SOD1*^{G93A}-Tg mouse spinal cord. Insets show higher magnification images of boxed area. Arrowheads indicate aggregate-like structures within motor neuron cell bodies, which were positive for both KAP3 and SOD1 (upper panel) and KAP3 and ubiquitin (lower panel). Scale bars = 50 μm.

ChAT supplied is more critical for the overall production of ACh (21). Therefore, to examine the impact of misfolded SOD1–KAP3 association on the function of motor neurons in *SOD1*^{G93A}-Tg mice during the disease progression, we decided to analyze the transport of ChAT in motor neurons. To achieve this, we obtained motor–cargo protein complexes using a previously described method from ventral roots of the caudal spinal cord, which represent motor axons just extended from the spinal cords and examined the presence of ChAT by immunoblot analysis. We found that a significantly lower level of ChAT was present in cauda equina of *SOD1*^{G93A}-Tg mice compared with those of *SOD1*^{WT}-Tg at 7 months of age or later (Fig. 3A). Furthermore, kinesin-2 motor components, KAP3, KIF3A and KIF3B, all showed a similar decrease in expression during the disease progression in cauda equina of *SOD1*^{G93A}-Tg mice. On the other hand, KHC (kinesin heavy chain), KLC (kinesin light chain) (kinesin-1 components) and Rab3 (a synaptic vesicle-associated protein transported by KIF1A) were consistently expressed during the disease progression. Decreased ChAT transport in pre-symptomatic *SOD1*^{G93A}-Tg mouse sciatic nerve was also demonstrated by a ligation assay (Supplementary Material, Fig. S2A). These results suggest that the amount of ChAT transported by the kinesin-2 complex significantly decreases in motor axons of *SOD1*^{G93A}-Tg mice prior to disease onset.

The results presented in Figure 2A show that ChAT does not co-migrate with the misfolded SOD1–KAP3 complex, suggesting that KAP3 does not bind to ChAT and misfolded SOD1 at the same time. Decreased amounts of ChAT and kinesin-2 motor complex within the axons of motor neurons in *SOD1*^{G93A}-Tg mice, together with Figure 2A data, suggest that the misfolded SOD1 species may inhibit kinesin-2-mediated ChAT transportation by trapping the kinesin-2 motor complex in the motor neuron cell body and the surrounding areas. For a better understanding of the misfolded SOD1 species behavior in motor axons of *SOD1*^{G93A}-Tg mice, we compared the migration profile in a sucrose density gradient centrifugation of kinesin motor components and ChAT with that of SOD1, by using the axonal motor-cargo protein complexes prepared above as a sample. We found that a small amount of misfolded SOD1 species are present in axonal motor–cargo protein complexes and co-migrate with a small fraction of KAP3, KIF3A (Fig. 3B) and KIF3B, although the detection of KIF3B requires very long exposure (data not shown). We also found that ChAT co-immunoprecipitates with KAP3 in fractions where KAP3 and kinesin-2 components co-migrated. (Supplementary Material, Fig. S2B). These results suggest that misfolded SOD1 species not only trap the kinesin-2 motor complex via association with KAP3 in and around the cell bodies but some of the misfolded SOD1 is also transported to axons in stead of normal cargos such as ChAT.

NG108-15 cells serve as an *in vitro* model for FALS

We showed a clear correlation between the association of misfolded SOD1 with KAP3 and the inhibition of ChAT transport within *SOD1*^{G93A}-Tg mouse motor axons. To examine the causal relationship between these two phenomena in detail, we developed a novel cell culture model for FALS, in which

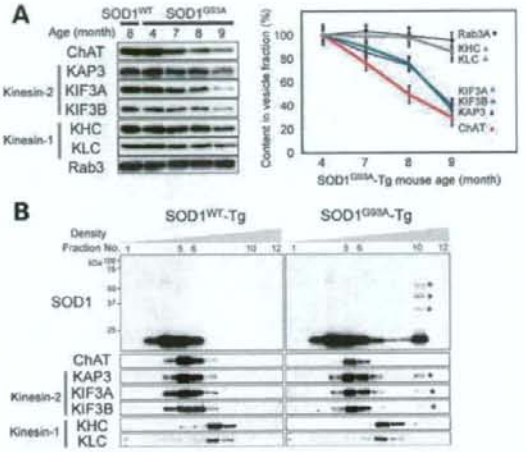

Figure 3. Axonal transport of ChAT was selectively impaired in spinal motor neurons preceding disease onset in SOD1^{G93A}-Tg mice. (**A**) Axonal transport components obtained from ventral roots from caudal spinal cords of *SOD1*^{WT}-Tg and *SOD1*^{G93A}-Tg mice at indicated ages were analyzed for the presence of indicated proteins by immunoblot analysis (left panel). The expression level of each molecule examined for *SOD1*^{G93A}-Tg mice is shown as a percentage of the level at 4 months of age (right panel). Note that the decrease in detection levels of ChAT and kinesin-2 components (KAP3, KIF3A and KIF3B) in *SOD1*^{G93A}-Tg mice became apparent at 7 months of age, 1 month before disease onset. (**B**) Fractions obtained from a sucrose density gradient centrifugation of axonal transported components from 8-month-old mice were analyzed for the presence of indicated proteins (SOD1 and individual components of kinesin motor complexes) by immunoblot analysis. Each lane (left to right) represents an aliquot collected from the top. Note that only kinesin-2 components co-migrated with misfolded SOD1 species (indicated by asterisks on the blots).

cells show cholinergic neuron-like properties—ChAT is transported within axon-like processes, ACh is released by depolarization and mutant SOD1 is misfolded/aggregated. For this purpose, we employed NG108-15 cells, which are of neuron/glia origin and known to differentiate into a cholinergic neuron-like phenotype (22,23). We first cloned a single cell-derived subline of NG108-15 cells, which we termed PNG3 (Purified NG108-15 cell-3), that showed highest expression of ChAT upon differentiation with dibutyryl cAMP and dexamethasone (data not shown). We observed that expression of ChAT and synaptophysin (an integral membrane protein found on synaptic vesicles) reaches the maximal level at ~72 h after the stimulation (Fig. 4A). By immunocytochemistry, we found that expression of ChAT and KAP3 were predominantly detected within the extended PNG3 processes in 72 h after the stimulation (Fig. 4B) as other kinesin-2 subunits (data not shown). From these observations, we decided to use PNG3 cells as a model for cholinergic neurons at day 3 after initiating differentiation for all the following experiments.

In order to use PNG3 cells as a cell line model for FALS, misfolding/aggregate formation by mutant SOD1 overexpression needs to be observed. Oxidative stress tends to cause mutant SOD1 proteins misfold and form aggregates (4). Experimentally, mutant SOD1 aggregate formation can be observed and facilitated by inhibiting proteasomal activity (24,25).

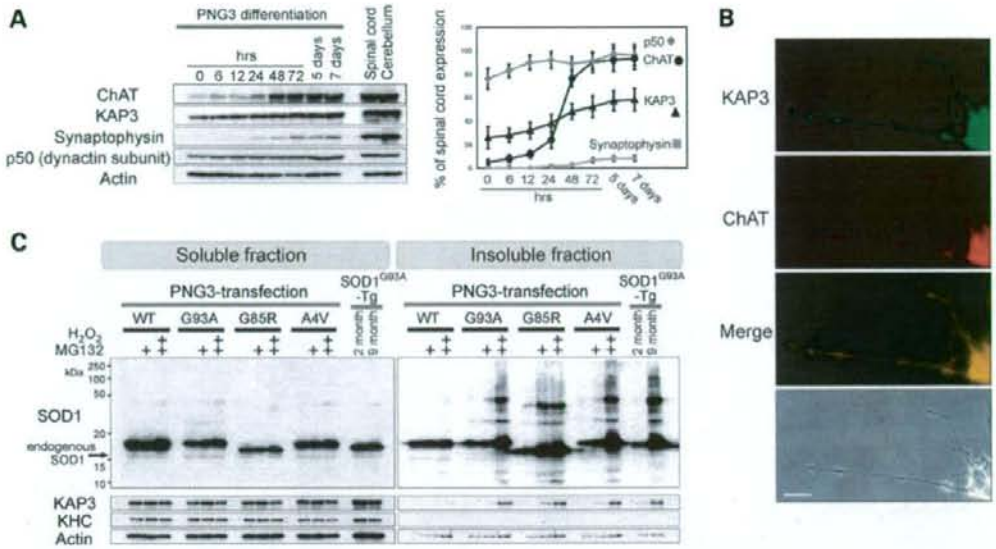

Figure 4. PNG3 cells served as an *in vitro* model system for studying mutant SOD1 toxicity on cholinergic neurons. (**A**) Expression of indicated proteins in PNG3 cells during cholinergic neuron-like differentiation was examined by immunoblot analysis. PNG3 cells were lysed at indicated times after induction of differentiation by dibutyryl cAMP and dexamethasone. Representative images of immunoblots (left panel) and quantitative analysis of the blots (right panel) are shown. Expression level is normalized to actin and relative to the level of normal spinal cord at each time point for each molecule. (**B**) Representative photographs of ChAT and KAP3 expression in differentiated PNG3 cell bodies and processes detected by immunocytochemistry are shown. Scale bar=25 μm. (**C**) Generation of misfolded SOD1 species in PNG3 cells overexpressing FLAG-tagged SOD1 bearing WT, G93A, G85R or A4V mutation was evaluated by immunoblot analysis. The transfected PNG3 cells were either untreated, treated by MG132 or treated by MG132 followed by H_2O_2 (as indicated above the images). One percent Triton X-100-soluble and -insoluble fractions were separately analyzed for SOD1-FLAG, KAP3, KHC and actin (for loading control). Spinal cords of 2- and 9-month-old *SOD1*^{G93A}-Tg mice were also subjected for the same set of analysis for comparison.

Therefore, we used a combined condition of increased oxidative stress plus decreased proteasomal activity to induce SOD1 misfolding and to enhance an accumulation of those misfolded SOD1 species in differentiated PNG3 cells overexpressing mutant SOD1. We transfected PNG3 cells with previously well-studied G93A, G85R and A4V mutations and wild-type control of human SOD1 for overexpression (3). Misfolded SOD1 species was detected in1% Triton X-100 insoluble fractions of lysates derived from all three types of FALS-linked SOD1 mutant transfectants but not in wild-type SOD1-overexpressing cells (Fig. 4C). We also found that SOD1 protein bearing the G85R mutation became misfolded without increasing oxidative stress, showing the previously reported unstable nature of this mutant protein (24). These results suggest that mutant SOD1 can form misfolded and/or aggregated molecules in differentiated PNG3 cells, very similar to what is seen in SOD1^{G93A}-Tg mice by pathological stresses.

For the analysis of pathological significance of misfolded SOD1–KAP3 association in this PNG3 cell model system, we next asked whether association of KAP3 with misfolded SOD1 is observed in this model just as we saw in the *SOD1*^{G93A}-Tg mice. To prove the association of KAP3 with misfolded SOD1 directly, we performed immunoprecipitation experiments using lysates of PNG3 cells transfected with either wild-type or mutant SOD1, and then treated with hydrogen peroxide to induce the mutant SOD1 misfolding. We found that anti-KAP3 immunoprecipitates contained misfolded SOD1 species, and the antibody against mutant SOD1-Flag immunoprecipitated misfolded SOD1 together with KAP3 (Fig. 5A). To visualize the misfolded SOD1-KAP3 association in PNG3 cells, we performed immunocytochemical analysis for localization of KAP3 and mutant SOD1. We found mutant SOD1-immunoreactive aggregates were prominent in cell bodies as well as the processes of MG132-treated differentiated PNG3 cells expressing G85R SOD1, and those aggregates were also positive for KAP3 (Fig. 5B and C). These observations together suggest that the cellular FALS model that we developed here using PNG3 cells recapitulates the association of KAP3 and misfolded SOD1 observed in *SOD1*^{G93A}-Tg mice and therefore is suitable to analyze the pathological impact of the misfolded SOD1-KAP3 association on motor neurons.

Microtubule-dependent fraction of depolarization-induced ACh release from PNG3 cells requires KAP3

In *Drosophila* neurons, the kinesin-2 motor complex is responsible for anterograde axonal transport of ChAT (18,19). To examine whether the same is true in mammals, we first developed an assay model to detect a depolarization-induced microtubule-dependent release of ACh as a result of ChAT transport. Differentiated PNG3 cells were metabolically

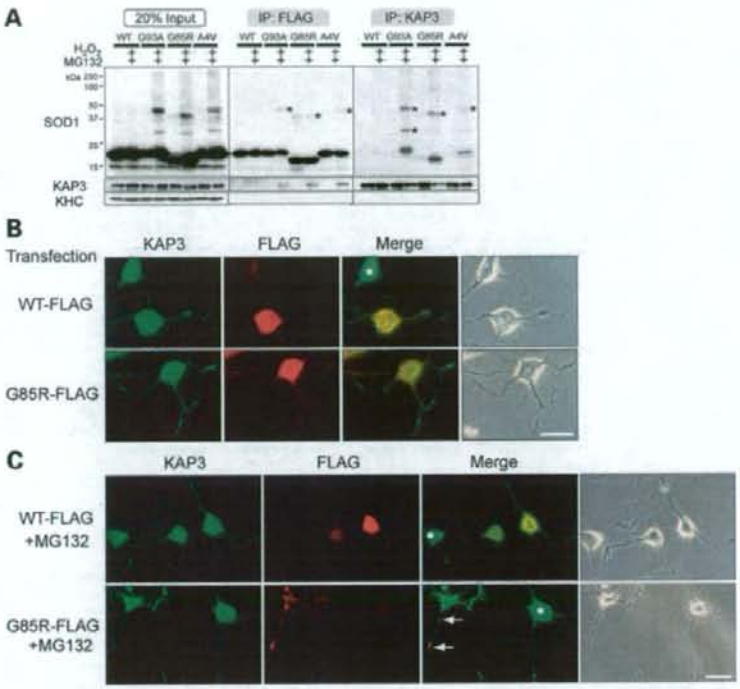

Figure 5. KAP3 associates with misfolded SOD1 species in differentiated PNG3 cells. (**A**) Immunoprecipitates of anti-FLAG and KAP3 antibodies (labeled as 'IP:FLAG' or 'IP:KAP3') from lysates of PNG3 cells transfected with expression plasmids for wild-type SOD1 or SOD1 with G93A, G85R or A4V mutation with or without induction of misfolding by MG132/H_2O_2 were analyzed for the presence of indicated proteins by immunoblot analysis. Immunoblot of lysates used for immunoprecipitation (20% of the amount) of the expression of the same set of proteins is also shown. Note that misfolded SOD1–KAP3 association was detected in all three mutant SOD1 transfectants (indicated by asterisks). (**B** and **C**) Photographs of KAP3 and FLAG-tagged SOD1 in differentiated PNG3 cells transfected with either FLAG-tagged wild-type SOD1 or SOD1 bearing a G85R mutation before and after MG132 treatment are shown in (B) and (C), respectively. Phase contrast images are also shown to the right of each set. Asterisks indicate untransfected cells. Note that prominent aggregate formation is only in the mutant SOD1-expressing cells and processes after MG132 treatment. Scale bars=25 μm.

labeled with [^{3}H]choline, and depolarization-induced [^{3}H]ACh release was measured. We observed that PNG3 cells released [^{3}H]ACh in a KCl dose-dependent manner (Fig. 6A). To distinguish 'nerve terminal' ACh release from exocytosis at other locations, we examined ACh release with and without colchicine, a microtubule destabilizing reagent that inhibits axonal transport (18). From ACh release experiments with different trial amounts of colchicine, we decided to use colchicine at 2.5 μM for the best differentiation of microtubule-dependent release representing the release from the terminal of differentiated PNG3 cellular processes. Treating the cells with this concentration converted nearly 20% of the tubulin from filamentous to free form in PNG3 cells (Supplementary Material, Fig. S3A). Then to analyze the involvement of KAP3/kinesin-2 in ChAT transport in the mammalian neuron using this assay system, we examined the effect of KAP3 mRNA down-regulation in differentiated PNG3 cells. Although NG108-15 cells are mouse–rat hybrid, transfection of siRNA for mouse KAP3 in PNG3 cells decreased the KAP3 protein level to ~15% after 2 days (Supplementary Material, Fig. S3B). We found that siRNA-mediated down-regulation of KAP3 significantly reduced the microtubule-dependent fraction of ACh release from PNG3 cells (Fig. 6B). This reduction in ACh release was rescued by the co-transfection of full-length human KAP3 which is not affected by the mouse siRNA we used. However, the ACh release was not rescued by the human KAP3 lacking C-terminal sequence (513–792 amino acids), which is required for the interaction with KIF3A/B (26). These results suggest that KAP3 is required for ChAT transport along microtubules and the subsequent release of ACh from nerve terminals in mammalian neurons.

As described above, we observed decreased ChAT axonal transport in *SOD1*^{G93A}-Tg mice. To examine whether misfolded SOD1 inhibits ChAT transport also in this FALS model system in culture, we measured microtubule-dependent ACh release from differentiated PNG3 cells after induced production of misfolded SOD1 species (procedure is summarized in Fig. 6C). We found that induction of SOD1 misfolding by MG132 treatment resulted in a significant decrease of microtubule-dependent ACh release from mutant SOD1-expressing PNG3, but not from wild-type SOD1-expressing cells

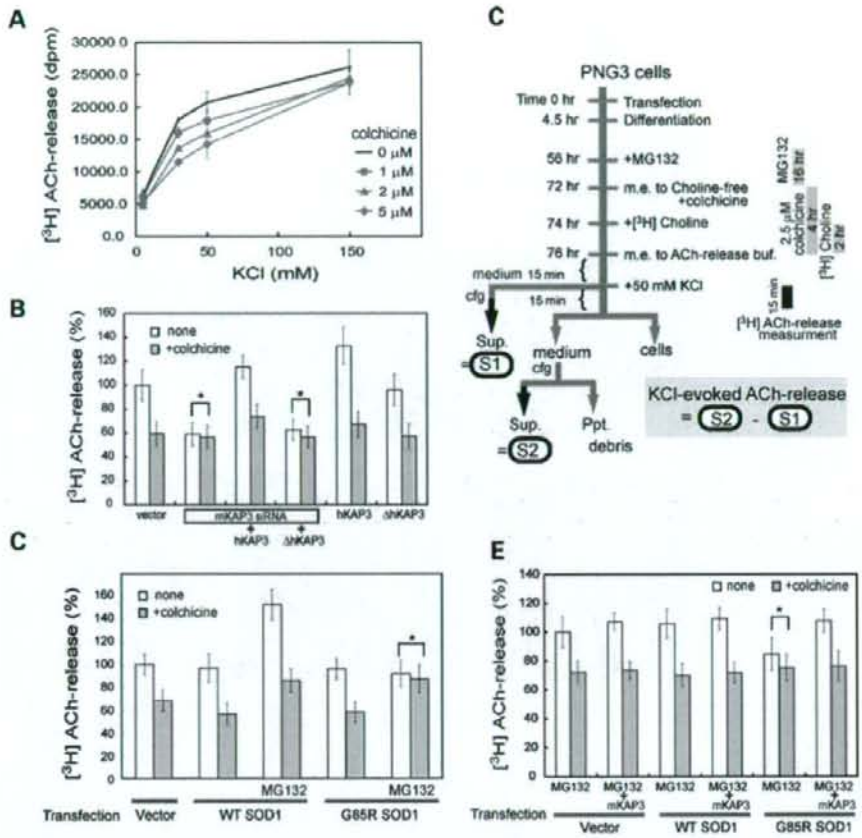

Figure 6. Microtubule-dependent fraction of depolarization-induced ACh release from PNG3 cells requires KAP3. (**A**) Differentiated PNG3 cells, metabolically labeled with [^{3}H]choline, were depolarized by increased KCl in the medium for 15 min. The radioactivity was released into the medium representing [^{3}H]ACh and was measured for different concentrations of KCl and colchicine, as indicated. (**B**) Depolarization-induced [^{3}H]ACh release from differentiated PNG3 cells transfected with vector only, siRNA for mouse KAP3 (mKAP3) or siRNA for mKAP3 together with expression plasmid for either human KAP3 (hKAP3) or hKAP3 lacking C-terminal 223 amino acids (ΔhKAP3), expression plasmid for hKAP3 only or expression plasmid for ΔhKAP3 was determined with or without colchicine treatment. Radioactivity is shown as a percentage to that from vector-transfected, colchicine-untreated cells. The asterisk indicates non-significant differences calculated as $P > 0.05$. Note that KAP3 down-regulation inhibited microtubule-dependent ACh release. (**C**) Summarized time schedule for [^{3}H]ACh-release measurement in differentiated PNG3 cells with and without SOD1 misfolding/aggregation. KCl-evoked release of ACh was calculated by subtracting the radioactivity in S1 (medium before KCl addition) from that in S2 (medium after KCl addition). (**D**) Depolarization-induced [^{3}H]ACh release from differentiated PNG3 cells transfected with vector only, expression plasmid for wild-type SOD1 or G85RSOD1 was determined with or without MG132 treatment. Microtubule-dependent and -independent fractions of release were measured for each condition analyzed. Radioactivity is shown as percentage to that from vector-transfected, colchicine-untreated cells. Note that ACh release from mutant SOD1-transfected cells was reduced in response to MG132 treatment, while overexpression of mutant SOD1 *per se* did not affect choline incorporation into cells (Supplementary Material, Fig. S4C). The asterisk indicates non-significant difference calculated as $P > 0.05$. (**E**) Depolarization-induced [^{3}H]ACh release from differentiated PNG3 cells transfected with vector only, expression plasmid for wild-type SOD1 or G85RSOD1, with or without co-transfection of mKAP3 expression plasmid, was determined after MG132 treatment. Microtubule-dependent and -independent fractions of release were measured for each condition analyzed. Radioactivity is shown as a percentage of that from vector-transfected, colchicine-untreated cells. Note that the reduction in ACh release observed in mutant SOD1-transfected cells in response to MG132 treatment was normalized by mKAP3 expression. The asterisk indicates non-significant difference calculated as $P > 0.05$.

(Fig. 6D, asterisk). MG132 treatment itself resulted in up-regulation of both microtubule-dependent and -independent ACh release (Fig. 6D and Supplementary Material, Fig. S4A). However, this MG132-induced increase in ACh release was presumably caused by increased expression levels of proteins necessary for ACh synthesis/release and was independent from the misfolded SOD1-induced effect (Supplementary Material, Figs S4B and C). These results suggest that misfolded SOD1 inhibits ChAT transport in this FALS model system in culture as well.

The observations in *SOD1^{G93A}*-Tg mice, as well as in the cellular FALS model system that we described, further

suggest that misfolded SOD1 causes a reduction or depletion of the functional kinesin-2 complex via its association with KAP3. This raises the possibility that misfolded SOD1-induced reduction in ChAT transport may be normalized by supplementing motor neurons with KAP3. To prove this hypothesis using the FALS culture model system, we examined microtubule-dependent ACh release from differentiated PNG3 cells overexpressing wild-type or mutant SOD1 together with KAP3. Overexpression of KAP3 did not change ACh release from MG132-treated PNG cells transfected with empty vector or wild-type SOD1. However, overexpression of KAP3 was able to normalize the ACh release reduction under the condition that causes mutant SOD1 misfolding (Fig. 6E). These results strongly suggest that misfolded SOD1-induced reduction in ChAT transport and ACh release is mediated by a reduction in functional KAP3 molecule because of its association with misfolded SOD1. These results may also suggest that the normalization of functional KAP3 level in motor neurons could have a therapeutic effect on FALS pathogenesis.

KAP3 was co-localized with mutant SOD1 aggregates within LBHI in spinal motor neurons from human FALS patients

As described, we performed analysis of the misfolded SOD1-induced reduction of ChAT transport in cultured cells in cultured cells as well as in a mouse model. To gain insight into the significance of this mechanism in human FALS, we performed immunohistochemistry on spinal cord sections of human SOD1-linked FALS cases to examine co-localization of KAP3 and SOD1. The neuropathological phenotypes of four patients we analyzed, who were members of two different families (27–29), are summarized in a table in Figure 7. These patients often developed Lewy-body-like hyaline inclusions (LBHIs), which are protein aggregates containing mutant/wild-type SOD1 and one of the most characteristic cytopathological changes in the spinal motor neurons of mutant *sod1*-linked FALS (28). Immunohistochemical analysis revealed that most of the LBHIs in the spinal motor neurons were positive for both KAP3 and SOD1 (arrowheads in Fig. 7). We confirmed that the KAP3 signal in LBHIs was not present when the anti-KAP3 antibody was pre-incubated with an excess of the synthetic KAP3 antigen peptides (data not shown). These observations demonstrated that KAP3–SOD1 interaction and subsequent co-aggregation frequently occurs in human SOD1-linked FALS cases.

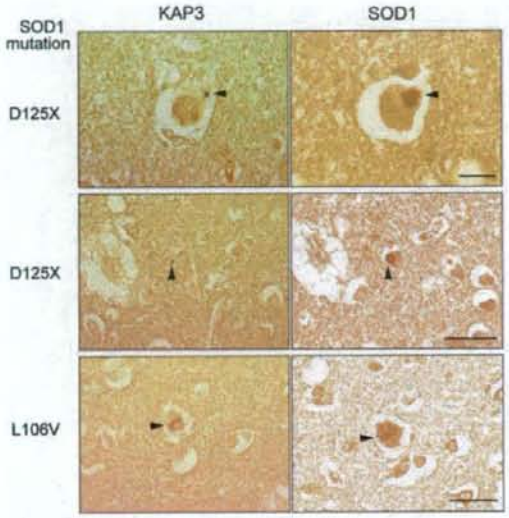

Neuropathological findings in autopsied patients with FALS examined.

SOD1 mutation	Number of patients	Neuronal inclusion	SOD1 aggregation	Bunina body	Corticospinal tract involvement	Posterior column involvement
D125X	2	LBHI	+	-	+	+
L106V	2	LBHI	+	-	+	+

+: present, -: absent, LBHI: Lewy-body-like hyaline inclusion

Figure 7. KAP3 was co-localized with SOD1 aggregates within LBHI in spinal motor neurons from human FALS cases. Consecutive sections of LBHI-containing spinal motor neurons from FALS patients possessing *sod1* mutations were immunostained with anti-KAP3 and anti-SOD1 antibodies. The clinicopathological characteristics of the FALS patients are summarized in the table. D125X mutation is a deletion of two nucleotides at codon 126 that results in the truncation of five residues downstream. Co-localization of KAP3 and SOD1 within the LBHI is evident (arrowheads). The images are representative of 30 LBHIs observed in each case, all of which showed co-localization of SOD1 and KAP3. Scale bars=25 μm for the images of top row, 50 μm in others.

DISCUSSION

In this paper, we presented a novel pathological mechanism by which misfolded SOD1 may cause neuronal dysfunction in FALS. A significant proportion of misfolded SOD1 is located within motor axons prior to disease onset in *SOD1*^{G93A}-Tg FALS model mice. We showed that misfolded SOD1 species selectively binds to KAP3 (Fig. 2B and C) and that this binding may be a cause for the reduction in functional KAP3 molecule required for kinesin-2-dependent transport within motor axons (Fig. 3A and B). The kinesin-2 motor complex is particularly important, because it is required for ChAT transport (19). Decreased ChAT expression and resultant decrease in ACh release from motor nerve ends can lead to dysfunction of motor synapses at axon terminals (30,31). By employing a newly developed cell culture model of FALS, we showed that ACh release from nerve terminals was decreased presumably due to a reduction in ChAT transport resulting from KAP3 sequestration by misfolded SOD1 species (Figs 5A and C and 6D). The pathological mechanism we propose from our data is schematized in Figure 8.

ALS-like motor neuron pathology is observed in transgenic mice expressing C-terminal truncated SOD1 (L126Z), in which the mutant SOD1 expression was not clearly observed in sciatic nerve (32). This suggests that KAP3-misfolded SOD1 association is formed mostly in motor neuron cell bodies. Indeed, we detected KAP3-misfolded SOD1 associ-

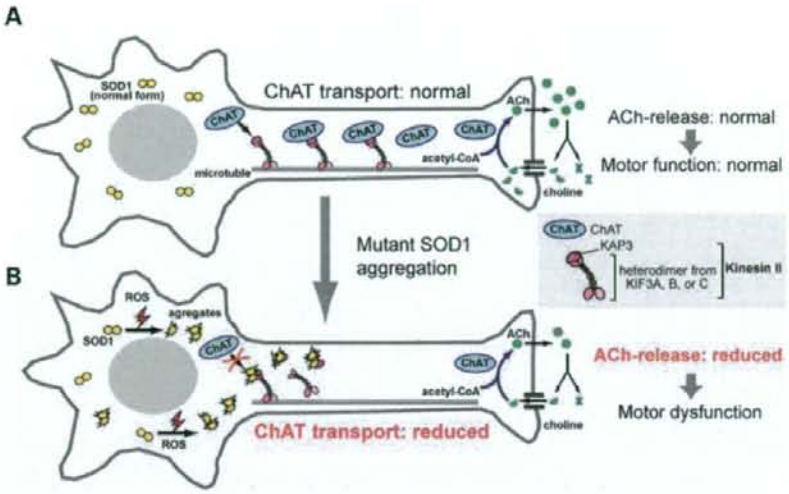

Figure 8. A schematic diagram for a mutant SOD1 toxicity and impairment of axonal transport of ChAT. In healthy motor neurons (**A**), ChAT is continuously transported by kinesin-2 motor, comprising KIF3A, KIF3B/C and KAP3, toward the neuromuscular junction where ACh functions as a neurotransmitter. ACh is released into the synaptic cleft upon stimulation and rapidly degraded into choline and acetic acid by AChE. Choline is taken up into the nerve terminal by choline transporters and then ChAT synthesizes ACh from choline and acetyl-CoA. The reaction catalized by ChAT is the rate-limiting step for ACh supply to the nerve terminals. In motor neurons expressing mutant SOD1 (**B**), mutant SOD1 proteins were converted into misfolded forms as a result of increased ROS generation and/or reduced proteasomal activity. Certain misfolded species preferentially binds to KAP3 and inhibit the binding of ChAT to KAP3, thereby causing a decrease in ChAT transport. This decrease in ChAT in the nerve terminals can constitute a mechanism that causes motor dysfunction.

ation in spinal cords (Fig. 2C) and ventral white matter (Fig. 2A and B) of *SOD1*^{G93A}-Tg mice prior to disease onset, but could not detect it in distal sciatic nerve even at the end-stage (data not shown). These findings suggest that, even if misfolded SOD1 associates with molecular motors, it cannot travel for a long distance, presumably because it is not a physiological cargo.

We suspect that misfolded SOD1–KAP3 association is one of the early events in FALS pathogenesis. Evidence to support this possibility is that the SOD1–KAP3 association becomes detectable around 6 months of age in *SOD1*^{G93A}-Tg mice, 2 months earlier than disease onset (Fig. 2C), suggesting that the SOD1–KAP3 association constitutes an early event in FALS motor neurons. Also, our immunoprecipitation/immunoblot analysis shows that SOD1–KAP3 association always detected relatively low molecular-weight misfolded SOD1 (−50 kDa) among all of the misfolded products ranging up to hundreds of kilodaltons in size (Figs 2B and C and 5A). The preferential association of KAP3 for low molecular-weight species but not with large precipitates suggests that SOD1–KAP3 association accounts for a fraction of the initial events in FALS pathogenesis. Previous reports on selective increase in KAP3 transcription in lumbar spinal cords from *SOD1*^{G86R}-Tg mice as an early event prior to disease onset (33) also supports our hypothesis, as the increase may be regarded as compensatory to the KAP3 sequestration by SOD1–KAP3 association.

Previous reports show that crossing mutant SOD1-Tg mice with dynein heavy chain mutant mice (*loa* or *cra*) delays the disease onset and extends survival (34,35). This result is surprising because mutations in dynein heavy chain, a subunit of dynein motor complex, or p150^{Glued}, a subunit of dynactin (dynein activator) cause dysfunction and degeneration of spinal motor neurons (15,16). This suggests a possible mechanistic link between impaired axonal transport in mutant *SOD1*-Tg mice and that in dynein heavy chain mutant mice. Here we demonstrated that KAP3 sequestration by misfolded SOD1 is a mechanism for selective inhibition of axonal transport observed in mutant SOD1-Tg mice. Previous reports on melanophore transport in *Xenopus* melanosomes showed that dynactin serves as an activator of kinesin-2 via direct binding of p150^{Glued} to KAP3 and regulates the intracellular direction of melanosome transport by binding to either dynein (retrograde) or KAP3 (anterograde) (36). Dynein and KAP3 share the same binding site on p150^{Glued}, and so p150^{Glued} binds to only one of them at a time and thereby activates transport in only one direction. If a similar regulation by dynactin plays a role in mammalian neurons, *loa* and *cra* mutations may increase the chance of p150^{Glued} to bind to KAP3, because those mutations promote subunit disassembly and increase dynein-unbound dynactin (15). By this mechanism, dynein heavy chain mutations may result in normalizing kinesin-2-mediated transport of ChAT inhibited by the misfolded SOD1 species. Indeed, in our analysis of ventral white matter in *SOD1*^{G93A}-Tg mice using Nycodenz density gradient centrifugation, a small fraction of p150^{Glued} co-migrated with misfolded SOD1 species and KAP3 (Fig. 2A). This population of p150^{Glued} also co-precipitated with KAP3 (data not shown). This result may reflect an involvement of p150^{Glued} in KAP3/SOD1 misfolding and aggregation through its interaction with KAP3.

A recent study provides an interesting evidence that transcription of all members of the KIF3 family selectively decreases in motor cortex of sporadic ALS patients among 13 kinds of kinesin and kinesin-related proteins (37). Impaired neuromuscular transmission was detected in early sporadic ALS patients (38), and a reduced supply of releasable ACh was thought to be the primary cause for the degeneration of motor terminal in a dog model of hereditary spinal muscular atrophy (30,39). It is possible that kinesin-2 dysfunction and subsequent inhibition of ChAT transport might be one of the common pathways leading to motor neuron-specific dysfunction in both sporadic and familial ALS cases.

The cargos and adaptor molecules for kinesin-2 have not been well studied. Small GTP-binding protein dissociation factor SmgGDS (40), fodrin (41), a tumor suppressor adenomatous polyposis coli (42), N-cadherin (43), ChAT and AChE (18) have been reported as molecules that bind to KAP3. Our finding that misfolded SOD1 species sequesters KAP3 raises a possibility that the transport of these molecules may also be impaired in mutant SOD1-related FALS, together with the reduced ChAT transport. Indeed, we observed a slight decrease in N-cadherin transport in motor axons from presymptomatic $SOD1^{G93A}$-Tg mice (Supplementary Material, Fig. S5). The expression and function of those molecules within motor neurons need to be studied to elucidate the entire mechanism.

MATERIALS AND METHODS

All the data in Figures 1–6 are a representative of three mice per group or three independent experiments. Statistical significance was assessed by ANOVA followed by Fisher's test. Error bars in graphs represent standard deviations. Signals in immunoblots were detected using ECL (GE Healthcare) and quantified with NIH image software (1.61J).

Reagents

All four types (WT, G93A, G85R and A4V) of FLAG-tagged human SOD1 cDNA at the C terminus were cloned into pcDNA3 (44). Full-length mouse (Image clone ID: 5698182) and human (4829354) KAP3 were purchased from Image clone bank and cloned into pcDNA3 and pCMV-Tag1, respectively. The integrity of each clone was verified by nucleotide sequence analysis. The siRNA designed for silencing mouse KAP3 (M-047278-00-0010) was purchased from Dharmacon Research. Primary antibodies used for immunoblots were as follows: anti-SOD1 (Stressgen, SOD-100, and Calbiochem, 574597), kinesin C2 (Affinity BioReagents) and CRMP-2 (Immuno-Biological Laboratories). Anti-ChAT (AB144P), KHC (MAB1614), KLC (MAB1617), synaptophysin (MAB5258-20UG), actin (MAB1501), Neurofilament-M (AB1987) and MBP (myelin basic protein, AB9046) antibodies were all purchased from Chemicon. Anti-KAP3, KIF3A, KIF3B, $p150^{Glued}$, p50 dynamitin, dynein IC, KIF2 and Rab3 antibodies were purchased from BD PharMingen/Transduction Laboratories. Primary antibodies used for immunoprecipitation and immunostaining were anti-SOD1 (Stressgen, SOD-100), ChAT (Chemicon, AB144P) and FLAG (Sigma, F3165) antibodies. KAP3 antibody was prepared by immunizing rabbits with a peptide containing the 1–14 amino acids of mouse KAP3, which are conserved in human KAP3, followed by affinity purification using an epitope-conjugated column.

Animals

We used the G1L line of transgenic mice harboring the G93A-mutated human *SOD1* gene (B6SJL-*TgN*(*SOD1-G93A*)1Gur[tl]) purchased from the Jackson Laboratories. Mice harboring wild-type human *SOD1* gene (B6.Cg-*Tg*(*SOD1*)2Gur/J) was a gift from Dr Kawamata of Kyoto University. C57BL/6J mice were also used. The transgenic mice were backcrossed with C57BL/6J for more than 14 generations. All data were derived from male mice. All the animal experiments were approved by the Animal Care Committee of National Center of Neurology and Psychiatry (NCNP).

Preparation of subsegments from mouse spinal cords using LMD technique

Frozen sections from mouse spinal cords were prepared without fixation and processed through AS LMD (Leica) as previously described (17). Five sections were pooled for each sample location for subsequent analyses.

Isolation of misfolded SOD1 species from ventral white matter of spinal cords

The spinal cord was dissected from the indicated mice, and the ventral half of white matter at L1-S3 level was carefully dissected under a microscope. The dissected samples were homogenized in 300 μl of Nz homogenization buffer [20 mM HEPES, pH 7.4, 120 mM NaCl, 2 mM EDTA, pH 8.0, 0.25% NP-40 and complete protease inhibitor cocktail (Roche)] followed by a brief sonication., The lysates were added to 3.2 ml of Nycodenz linear density gradient in 10 mM HEPES, pH 7.4 and 1 mM EDTA, pH 8.0 (initial concentration of Nycodenz was 30%). After a centrifugation at 87 479g for 2 h at 4°C, in Optima MAX-E using MLS 50 rotor (Beckman Coulter), 160 μl of aliquot was collected from the top to the bottom of the tube, totaling 22 fractions. Twenty microliters of each fraction was collected and analyzed by immunoblot.

Immunoprecipitation

Affinity-purified anti-KAP3 and anti-SOD1 antibodies were captured with Dynabeads Protein G (Dynal Biotech) and cross-linked using dimethyl pimelimidate as per manufacturer's protocol. For the immunoprecipitation from fractions prepared from Nycodenz density gradient centrifugation, 30 μl of each fraction was mixed with the antibody-conjugated Dynabeads in 20 mM HEPES, pH 7.4, 120 mM NaCl, 2 mM EDTA and complete protease inhibitor cocktail. The mixture was incubated overnight at 4°C on a rocking platform, followed by washing with PBS containing 0.05% Tween-20. The target proteins were eluted with 30 μl of 0.1 M citric acid (pH 2.0) for 2 min, and half of the eluates

were analyzed. For the immunoprecipitation from spinal cords or SOD1-transfected PNG3 cells, tissues or cells were lysed in TN-T buffer (50 mM Tris–HCl, pH 7.6, 1% Triton X-100, 150 mM NaCl) containing complete protease inhibitor cocktail and subjected to a centrifugation at 5000*g* for 10 min at 4°C. The supernatants were incubated with antibody-conjugated Protein G Dynabeads and analyzed as described above.

Preparation of transported components from ventral cauda equina

The fraction enriched with transported components within motor axons was prepared from ventral roots of caudal spinal cords as described (41) with the following modifications. Ventral cauda equina was minced for two times in 400 μl of IM-D buffer supplemented with 1 mM ATP and a protease inhibitor cocktail (Complete; Roche) for 10 min on ice. They were subsequently subjected to centrifugation at 5000*g* for 10 min at 4°C. The obtained supernatants were measured for protein concentration and 5 μg of each was subjected to SDS/PAGE to evaluate the kinesin-2 contents. To analyze kinesin-2 status, the transported vesicle fractions prepared from four mice were subjected to 4.4 ml of sucrose step gradient centrifugation ranging from 0.2 to 2%. After centrifugation in an SW55 Ti rotor (Beckman Coulter) at 50 000 rpm for 18 h at 4°C, 400 μl of each fraction was collected from top of the tube, totaling 12 fractions, and 20 μl of each fraction was analyzed by SDS–PAGE/immunoblots.

Cell culture and transfection

NG108-15 cells (a kind gift from Dr Akazawa in Tokyo Medical and Dental University), a hybrid cell line of mouse N18TG2 neuroblastoma cells and rat C6-BU-1 glioma cells, were cultured in Dulbecco's modified Eagle's medium (DMEM) (Sigma, D5796) containing 10% fetal bovine serum and 2% HAT supplement (GIBCO). Differentiation of PNG3, a subclone of NG108-15 isolated from single cells, was induced with 1 mM of dibutyryl cAMP (Nacalai tesque) and 0.2 μM of dexamethasone (MB Biomedicals) for 3 days. Transfection of plasmids into PNG3 was performed using Optifect or Lipofectamine 2000 (Invitrogen Life Technologies) as per manufacturer's protocol. Culture medium was changed every 20–24 h except where indicated otherwise. Transfection of siRNA and co-transfection of siRNA with plasmids were performed according to the manufacturer's protocols using DharmaFECT transfection reagent 2 (Dharmacon) and DharmaEFCT Duo transfection reagent, respectively. For induction of SOD1 misfolding/aggregation, cells were treated with 6.5 μM of MG132 (a proteasome inhibitor) 56 h after transfection and then treated with 2.5 mM hydrogen peroxide for 2 h at 72 h after transfection. Cells were then lysed with TN-T buffer plus Complete protease inhibitor cocktail and subjected to centrifugation at 10 000*g* for 10 min at 4°C to be separated into soluble (supernatant) and insoluble (pellet) fractions.

Measurement of [^{3}H]ACh release

Depolarization-induced [^{3}H]ACh release was measured based on the method previously described (Kumagai *et al.*, 1993) with several modifications. For metabolic labeling of PNG3 cells by [^{3}H]choline, DMEM lacking choline chloride was used. Time schedules for labeling, reagents used and incubation time are shown in Figure 6C.

The culture medium was changed to choline-free DMEM either with or without colchicine. After 2 h incubation, 6.25 kBq [^{3}H]choline chloride ([methyl-^{3}H] choline chloride, 2.2 TBq/mmol; GE Healthcare) was added to the medium of each well of a 12-well plate. After 2 h incubation, the medium was changed to ACh release measuring buffer [20 mM HEPES-NaOH, pH 7.4, 150 mM NaCl, 5 mM KCl, 1.8 mM $CaCl_2$, 0.8 mM $MgSO_4$, 25 mM glucose, 25 μM eserine sulfate and 10 μM hemicholinium-3 (HC-3)] and the culture plates were returned to the CO_2 incubator. Eserine, an inhibitor for cholinesterase, was added to inhibit a degradation of released ACh by cholinesterase. HC-3, an inhibitor for high-affinity choline transporter 1, was added to completely inhibit [^{3}H]choline uptake after changing the medium. After 15 min incubation, with eserine and HC-3, an aliquot of culture medium was transferred into a 1.5 ml tube (media before KCl addition), and then KCl was added into the medium to a final concentration of 50 mM. The culture plates were quickly returned to the CO_2 incubator, and after 15 min, the medium was transferred into a new 1.5 ml tube (media after KCl addition). Both the medium collected before and after KCl addition were centrifuged at 10 000*g* for 5 min at 4°C to remove debris. The supernatants were mixed with a scintillation cocktail (Ultima Gold XR, Perkin Elmer) to measure the [^{3}H] radioactivity using a liquid scintillation spectrophotometer. The radioactivity of [^{3}H]ACh released by KCl was calculated by subtracting the activity of media before KCl (=S1) from the activity of media after KCl addition (=S2), as described in Figure 6C.

Immunocytochemistry

PNG3 cells were fixed with 4% paraformaldehyde in PBS for 15 min. After permeabilization with 0.15% Triton X-100 in PBS for 10 min, cells were treated with Blocking-one (Nacalai) for 1 h. The cells were then treated with primary antibodies in Blocking-one at 4°C overnight. The cells were washed with PBS. For detection, cells were treated with fluorescent-conjugated secondary antibodies in Blocking-one at room temperature for 1 h. After washing again with PBS, cells were mounted with Vectasheld (Vector Laboratories).

Autopsy specimens and immunohistochemistry

The studies were performed on archival, buffered 10% formalin-fixed, paraffin-embedded spinal cord tissues obtained at autopsy from four FALS patients who were members of two different families. Consent for autopsy was obtained from legal representatives in accordance with the requirements of local institutional review boards. The clinicopathological characteristics of the FALS patients have been previously reported (27,29). SOD1 gene analysis revealed that the members of the Japanese Oki family had a 2 bp deletion at codon 126 in the gene for SOD1 (frame-shift 126 mutation, D125X) and that the members of the T family had a Leucine to Valine substitution at codon 106 in the SOD1

gene (L106V). To look at the expression of KAP3 and SOD1 in these specimens, affinity-purified rabbit anti-KAP3 antibody (0.05 μg/ml, diluted 1:200 in 1% bovine serum albumin-containing PBS, pH 7.4), mouse monoclonal antibody against human SOD1 (0.5 mg/ml, clone1G_2, MBL, Aichi, Japan) and sheep polyclonal antibody against human SOD1 (1:20,000, Calbiochem, Darmstadt, Germany) were used as primary antibodies. Immunohistochemical reaction was performed by a standard procedure. Antibody signal was visualized by the avidin–biotin–immunoperoxidase complex (ABC) method using the appropriate Vectastain ABC Kit (Vector Laboratories, Burlingame, CA, USA) and 3,3′-diaminobenzidine tetrahydrochloride (DAB; Dako, Glostrup, Denmark) as the chromogen.

SUPPLEMENTARY MATERIAL

Supplementary Material is available at *HMG* online.

ACKNOWLEDGEMENTS

We wish to thank the laboratory members for helpful suggestions and Tomoko Dai, Mariko Soda, Yumiko Shimazaki and Tadatoshi Makino for their technical support.

Conflict of Interest statement. None declared.

FUNDING

This work was supported by research grants from RIKEN BSI, a Grant-in-Aid for Scientific Research on Priority Area (Advanced Brain Science Project) from the Ministry of Education, Culture, Sports, Science and Technology, NIBIO (Program for Promotion of Fundamental Studies in Health Sciences), a grant from Japan Foundation for Neuroscience and Mental Health and grants from the Ministry of Health, Labor and Welfare of Japan. Funding to pay the Open Access charge was provided by a grant from Ministry of Health, Labour and Welfare of Japan.

REFERENCES

1. Boillee, S., Vande Velde, C. and Cleveland, D.W. (2006) ALS: a disease of motor neurons and their nonneuronal neighbors. *Neuron*, **52**, 39–59.
2. Pasinelli, P. and Brown, R.H. (2006) Molecular biology of amyotrophic lateral sclerosis: insights from genetics. *Nat. Rev. Neurosci.*, **7**, 710–723.
3. Shaw, B.F. and Valentine, J.S. (2007) How do ALS-associated mutations in superoxide dismutase 1 promote aggregation of the protein? *Trends Biochem. Sci.*, **32**, 78–85.
4. Barber, S.C., Mead, R.J. and Shaw, P.J. (2006) Oxidative stress in ALS: a mechanism of neurodegeneration and a therapeutic target. *Biochim. Biophys. Acta.*, **1762**, 1051–1067.
5. Wang, J., Xu, G. and Borchelt, D.R. (2002) High molecular weight complexes of mutant superoxide dismutase 1: age-dependent and tissue-specific accumulation. *Neurobiol. Dis.*, **9**, 139–148.
6. Shibata, N., Asayama, K., Hirano, A. and Kobayashi, M. (1996) Immunohistochemical study on superoxide dismutases in spinal cords from autopsied patients with amyotrophic lateral sclerosis. *Dev. Neurosci.*, **18**, 492–498.
7. Watanabe, M., Dykes-Hoberg, M., Culotta, V.C., Price, D.L., Wong, P.C. and Rothstein, J.D. (2001) Histological evidence of protein aggregation in mutant SOD1 transgenic mice and in amyotrophic lateral sclerosis neural tissues. *Neurobiol. Dis.*, **8**, 933–941.
8. Jonsson, P.A., Graffmo, K.S., Andersen, P.M., Brannstrom, T., Lindberg, M., Oliveberg, M. and Marklund, S.L. (2006) Disulphide-reduced superoxide dismutase-1 in CNS of transgenic amyotrophic lateral sclerosis models. *Brain*, **129**, 451–464.
9. Koyama, S., Arawaka, S., Chang-Hong, R., Wada, M., Kawanami, T., Kurita, K., Kato, M., Nagai, M., Aoki, M., Itoyama, Y. *et al.* (2006) Alteration of familial ALS-linked mutant SOD1 solubility with disease progression: its modulation by the proteasome and Hsp70. *Biochem. Biophys. Res. Commun.*, **343**, 719–730.
10. Goldstein, L.S. and Yang, Z. (2000) Microtubule-based transport systems in neurons: the roles of kinesins and dyneins. *Annu. Rev. Neurosci.*, **23**, 39–71.
11. Hirokawa, N. and Takemura, R. (2005) Molecular motors and mechanisms of directional transport in neurons. *Nat. Rev. Neurosci.*, **6**, 201–214.
12. De Vos, K.J., Grierson, A.J., Ackerley, S. and Miller, C.C. (2008) Role of axonal transport in neurodegenerative diseases. *Annu. Rev. Neurosci.*, **31**, 151–173.
13. Collard, J.F., Cote, F. and Julien, J.P. (1995) Defective axonal transport in a transgenic mouse model of amyotrophic lateral sclerosis. *Nature*, **375**, 61–64.
14. Williamson, T.L. and Cleveland, D.W. (1999) Slowing of axonal transport is a very early event in the toxicity of ALS-linked SOD1 mutants to motor neurons. *Nat. Neurosci.*, **2**, 50–56.
15. Hafezparast, M., Klocke, R., Ruhrberg, C., Marquardt, A., Ahmad-Annuar, A., Bowen, S., Lalli, G., Witherden, A.S., Hummerich, H., Nicholson, S. *et al.* (2003) Mutations in dynein link motor neuron degeneration to defects in retrograde transport. *Science*, **300**, 808–812.
16. Puls, I., Jonnakuty, C., LaMonte, B.H., Holzbaur, E.L., Tokito, M., Mann, E., Floeter, M.K., Bidus, K., Drayna, D., Oh, S.J. *et al.* (2003) Mutant dynactin in motor neuron disease. *Nat. Genet.*, **33**, 455–456.
17. Tateno, M., Sadakata, H., Tanaka, M., Itohara, S., Shin, R.M., Miura, M., Masuda, M., Aosaki, T., Urushitani, M., Misawa, H. *et al.* (2004) Calcium-permeable AMPA receptors promote misfolding of mutant SOD1 protein and development of amyotrophic lateral sclerosis in a transgenic mouse model. *Hum. Mol. Genet.*, **13**, 2183–2196.
18. Baqri, R., Charan, R., Schimmelpfeng, K., Chavan, S. and Ray, K. (2006) Kinesin-2 differentially regulates the anterograde axonal transports of acetylcholinesterase and choline acetyltransferase in *Drosophila*. *J. Neurobiol.*, **66**, 378–392.
19. Ray, K., Perez, S.E., Yang, Z., Xu, J., Ritchings, B.W., Steller, H. and Goldstein, L.S. (1999) Kinesin-II is required for axonal transport of choline acetyltransferase in *Drosophila*. *J. Cell Biol.*, **147**, 507–518.
20. Hirokawa, N. (2000) Stirring up development with the heterotrimeric kinesin KIF3. *Traffic*, **1**, 29–34.
21. Blusztajn, J.K. and Wurtman, R.J. (1983) Choline and cholinergic neurons. *Science*, **221**, 614–620.
22. McGee, R., Simpson, P., Christian, C., Mata, M., Nelson, P. and Nirenberg, M. (1978) Regulation of acetylcholine release from neuroblastoma × glioma hybrid cells. *Proc. Natl Acad. Sci. USA*, **75**, 1314–1318.
23. Tojima, T., Yamane, Y., Takahashi, M. and Ito, E. (2000) Acquisition of neuronal proteins during differentiation of NG108-15 cells. *Neurosci. Res.*, **37**, 153–161.
24. Johnston, J.A., Dalton, M.J., Gurney, M.E. and Kopito, R.R. (2000) Formation of high molecular weight complexes of mutant Cu, Zn-superoxide dismutase in a mouse model for familial amyotrophic lateral sclerosis. *Proc. Natl Acad. Sci. USA*, **97**, 12571–12576.
25. Puttaparthi, K., Wojcik, C., Rajendran, B., DeMartino, G.N. and Elliott, J.L. (2003) Aggregate formation in the spinal cord of mutant SOD1 transgenic mice is reversible and mediated by proteasomes. *J. Neurochem.*, **87**, 851–860.
26. Haraguchi, K., Hayashi, T., Jimbo, T., Yamamoto, T. and Akiyama, T. (2006) Role of the kinesin-2 family protein, KIF3, during mitosis. *J. Biol. Chem.*, **281**, 4094–4099.
27. Kato, S., Shimoda, M., Watanabe, Y., Nakashima, K., Takahashi, K. and Ohama, E. (1996) Familial amyotrophic lateral sclerosis with a two base pair deletion in superoxide dismutase 1: gene multisystem degeneration with intracytoplasmic hyaline inclusions in astrocytes. *J. Neuropathol. Exp. Neurol.*, **55**, 1089–1101.
28. Kato, S., Hayashi, H., Nakashima, K., Nanba, E., Kato, M., Hirano, A., Nakano, I., Asayama, K. and Ohama, E. (1997) Pathological

characterization of astrocytic hyaline inclusions in familial amyotrophic lateral sclerosis. *Am. J. Pathol.*, **151**, 611–620.
29. Kato, S. (2008) Amyotrophic lateral sclerosis models and human neuropathology: similarities and differences. *Acta Neuropathol.*, **115**, 97–114.
30. Rich, M.M., Wang, X., Cope, T.C. and Pinter, M.J. (2002) Reduced neuromuscular quantal content with normal synaptic release time course and depression in canine motor neuron disease. *J. Neurophysiol.*, **88**, 3305–3314.
31. Brandon, E.P., Lin, W., D'Amour, K.A., Pizzo, D.P., Dominguez, B., Sugiura, Y., Thode, S., Ko, C.P., Thal, L.J., Gage, F.H. *et al.* (2003) Aberrant patterning of neuromuscular synapses in choline acetyltransferase-deficient mice. *J. Neurosci.*, **23**, 539–549.
32. Wang, J., Xu, G., Li, H., Gonzales, V., Fromholt, D., Karch, C., Copeland, N.G., Jenkins, N.A. and Borchelt, D.R. (2005) Somatodendritic accumulation of misfolded SOD1-L126Z in motor neurons mediates degeneration: alphaB-crystallin modulates aggregation. *Hum. Mol. Genet.*, **14**, 2335–2347.
33. Dupuis, L., de Tapia, M., Rene, F., Lutz-Bucher, B., Gordon, J.W., Mercken, L., Pradier, L. and Loeffler, J.P. (2000) Differential screening of mutated SOD1 transgenic mice reveals early up-regulation of a fast axonal transport component in spinal cord motor neurons. *Neurobiol. Dis.*, **7**, 274–285.
34. Teuchert, M., Fischer, D., Schwalenstoecker, B., Habisch, H.J., Bockers, T.M. and Ludolph, A.C. (2006) A dynein mutation attenuates motor neuron degeneration in SOD1(G93A) mice. *Exp. Neurol.*, **198**, 271–274.
35. Kieran, D., Hafezparast, M., Bohnert, S., Dick, J.R., Martin, J., Schiavo, G., Fisher, E.M. and Greensmith, L. (2005) A mutation in dynein rescues axonal transport defects and extends the life span of ALS mice. *J. Cell Biol.*, **169**, 561–567.
36. Deacon, S.W., Serpinskaya, A.S., Vaughan, P.S., Lopez Fanarraga, M., Vernos, I., Vaughan, K.T. and Gelfand, V.I. (2003) Dynactin is required for bidirectional organelle transport. *J. Cell Biol.*, **160**, 297–301.
37. Pantelidou, M., Zographos, S.E., Lederer, C.W., Kyriakides, T., Pfaffl, M.W. and Santama, N. (2007) Differential expression of molecular motors in the motor cortex of sporadic ALS. *Neurobiol. Dis.*, **26**, 577–589.
38. Maselli, R.A., Wollman, R.L., Leung, C., Distad, B., Palombi, S., Richman, D.P., Salazar-Grueso, E.F. and Roos, R.P. (1993) Neuromuscular transmission in amyotrophic lateral sclerosis. *Muscle Nerve*, **16**, 1193–1203.
39. Balice-Gordon, R.J., Smith, D.B., Goldman, J., Cork, L.C., Shirley, A., Cope, T.C. and Pinter, M.J. (2000) Functional motor unit failure precedes neuromuscular degeneration in canine motor neuron disease. *Ann. Neurol.*, **47**, 596–605.
40. Shimizu, K., Kawabe, H., Minami, S., Honda, T., Takaishi, K., Shirataki, H. and Takai, Y. (1996) SMAP, an Smg GDS-associating protein having arm repeats and phosphorylated by Src tyrosine kinase. *J. Biol. Chem.*, **271**, 27013–27017.
41. Takeda, S., Yamazaki, H., Seog, D.H., Kanai, Y., Terada, S. and Hirokawa, N. (2000) Kinesin superfamily protein 3 (KIF3) motor transports fodrin-associating vesicles important for neurite building. *J. Cell Biol.*, **148**, 1255–1265.
42. Jimbo, T., Kawasaki, Y., Koyama, R., Sato, R., Takada, S., Haraguchi, K. and Akiyama, T. (2002) Identification of a link between the tumour suppressor APC and the kinesin superfamily. *Nat. Cell Biol.*, **4**, 323–327.
43. Teng, J., Rai, T., Tanaka, Y., Takei, Y., Nakata, T., Hirasawa, M., Kulkarni, A.B. and Hirokawa, N. (2005) The KIF3 motor transports N-cadherin and organizes the developing neuroepithelium. *Nat. Cell Biol.*, **7**, 474–482.
44. Urushitani, M., Kurisu, J., Tsukita, K. and Takahashi, R. (2002) Proteasomal inhibition by misfolded mutant superoxide dismutase 1 induces selective motor neuron death in familial amyotrophic lateral sclerosis. *J. Neurochem.*, **83**, 1030–1042.
45. Kumagai-Tohda, C., Tohda, M. and Nomura, Y. (1993) Increase in neurite formation and acetylcholine release by transfection of growth-associated protein-43 cDNA into NG108-15 cells. *J. Neurochem.*, **61**, 526–532.